Journal of Materials Chemistry A

Accepted Manuscript

This article can be cited before page numbers have been issued, to do this please use: G. A. Mutch, L. Qu, G. Triantafyllou, W. Xing, M. Fontaine and I. S. Metcalfe, *J. Mater. Chem. A*, 2019, DOI: 10.1039/C9TA01979K.

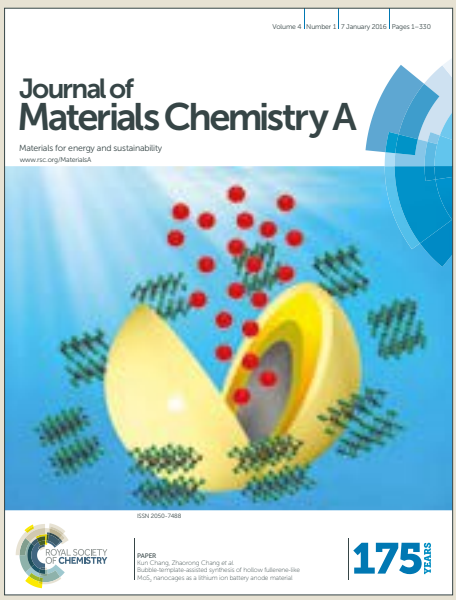

ROYAL SOCIETY OF CHEMISTRY

rsc.li/materials-a

View Article Online
DOI: 10.1039/C9TA01979K

Journal Name

ARTICLE

Supported molten-salt membranes for carbon dioxide permeation

Greg A. Mutch,[a] Liu Qu,[a] Georgios Triantafyllou,[a] Wen Xing,[b] Marie-Laure Fontaine[b] and Ian S. Metcalfe[a,*]

Received 00th January 20xx,
Accepted 00th January 20xx

DOI: 10.1039/x0xx00000x

www.rsc.org/

Membranes for selective carbon dioxide permeation are likely to be important devices in future separation processes relevant to the energy industry. Here we review the current state of research into a particular class of carbon dioxide permeable membrane: the supported molten-salt membrane. Such membranes rely upon ionic transport pathways through a molten salt with or without electronic and ionic transport contributions from the inorganic support. This variety of transport pathways allows a considerable degree of flexibility in membrane design. The use of molten salts permits high temperature operation and produces highly permeable membranes with theoretically infinite selectivity. Here we review work on materials selection and properties, likely permeation mechanisms and the role and control of membrane microstructure. We review results from permeation experiments and discuss the importance of materials compatibility and the role of interfacial processes in membrane degradation. We finish with comments on prospects for scale-up and commercialisation.

1. Introduction

To limit global warming to the commonly agreed 2°C scenario, overall negative emissions, *i.e.* a reduction in the atmospheric concentration of carbon dioxide, will likely be required.[1] Therefore, carbon dioxide separation from chemical reactions, flue gases and air will be needed. The scale of operation required to have a meaningful impact means that any carbon dioxide separation process will need to be economically and energetically low cost (separation processes already account for 10 - 15% of global energy consumption).[2] Carbon dioxide separation is currently achieved at commercial scale using absorption or adsorption "looping" technologies,[3] typically where there is an immediate end-use either for the carbon dioxide itself or for another component of the process stream, *e.g.* carbon dioxide separation in hydrogen production processes. However, to realise the targets set by climate change agreements, carbon dioxide separation will need to be exploited at a far larger scale in continuous, efficient, low-cost, robust and clean processes, with low energy penalties.

In principle, a membrane process could meet these requirements. Compared with ab/adsorption processes, membrane processes do not need temperature and/or pressure swings, lowering energy penalties and offering continuous operation. However, membranes require both high permeability (transport through the membrane) and high selectivity (selective separation of one component) to achieve efficient separation. This must be demonstrated continuously over long time periods using low-cost and environmentally-friendly materials. One class of membrane with potential to offer this combination, is the supported molten-salt membrane. For carbon dioxide permeation, a supported molten-salt membrane consists of a molten carbonate phase held within the pore space of a porous inorganic solid. Carbon dioxide selectivity is theoretically infinite, due to facilitated transport, and permeability is orders of magnitude higher than the dominant polymeric membrane class, due to liquid-like diffusion coefficients in the molten salt. The combination of a solid phase and a liquid phase offers flexibility in design and avoids issues with thermal expansion mismatch. Furthermore, pressurisation/evacuation of feed/permeate streams is not necessarily required to achieve a high transmembrane flux. This is a distinct advantage when applied to carbon dioxide separation, where compression costs are one of the primary difficulties to overcome.[4] Overall, these characteristics mean that in the longer term such membranes, although relatively new, are likely to compete with more established carbon dioxide permeable membrane technologies.

In this review we introduce the supported molten-salt membrane and discuss the fundamental materials chemistry of each component (molten salt and solid support) in the context of preparation and operation. Their combination and resulting permeation and materials compatibility properties are presented, largely focussed on carbon dioxide separation. We discuss commercialisation and scale-up before highlighting open questions that should be addressed to realise the potential of this promising class of membrane.

1.1 Status of Carbon Dioxide Separation Technologies

Commercial carbon dioxide separation (defined as >0.4 $MtCO_2$ captured annually) for the purpose of reducing emissions has been achieved in a very limited number of cases

[a] School of Engineering, Newcastle University, Newcastle, United Kingdom
[b] Sustainable Energy Technology, SINTEF, Oslo, Norway.
*Email - i.metcalfe@ncl.ac.uk

Electronic Supplementary Information (ESI) available: [details of any supplementary information available should be included here]. See DOI: 10.1039/x0xx00000x

View Article Online
DOI: 10.1039/C9TA01979K

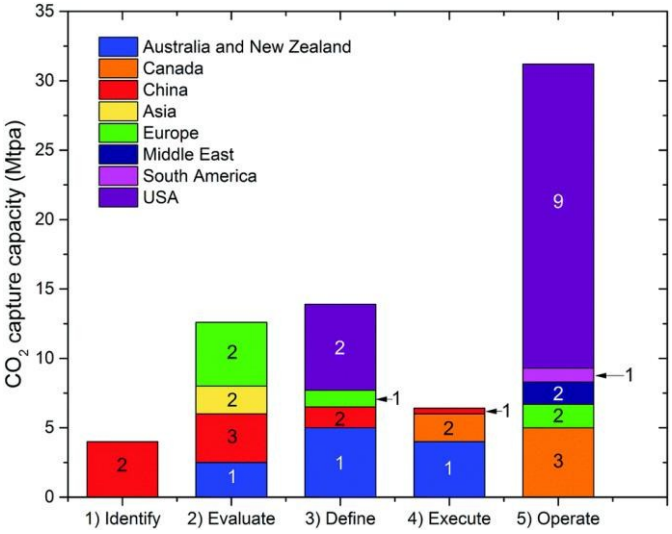

Fig. 1 – Worldwide carbon dioxide capture capacity of commercial-scale carbon dioxide separation projects (*i.e.* >0.4 $MtCO_2$ captured annually), in various stages of development: Identify - scoping and screening studies; Evaluate - conceptual design; Define - feasibility studies and front end engineering design; Execute - construction and commissioning; Operate - asset management. Number labels indicate the number of projects in each geographical region. Adapted from reference 3.

(Fig. 1).[3] The majority of current operations use the long-established aqueous amine absorbent looping approach,[5] to produce carbon dioxide for enhanced oil recovery. Amine absorbent processes suffer from high energetic penalties,[6] due to the high affinity of amines for carbon dioxide and the high heat capacity of the aqueous solution. Attempts to lower the energy requirement for regeneration have led to the creation of proprietary amine solutions. Research efforts have also focussed on replacing solvent absorbents with solid adsorbents, to lower the energy requirement further.[7]

Demonstrations of carbon dioxide adsorbent separation processes, distinguished from the commercial operations mentioned above in terms of scale (*i.e.* <0.4 $MtCO_2$ captured annually), include the use of metal oxides,[8,9] hydrotalcites[10] and zeolites.[11] Recently, direct capture of carbon dioxide from air has been demonstrated, using solid-supported amine adsorbents,[12,13] and combined aqueous hydroxide and solid metal oxide loops.[14] Overall, an extensive range of materials has been investigated for their carbon dioxide adsorption properties and application in separation processes.[7,15]

Membrane separation of carbon dioxide is also at demonstration level, with polymeric Polaris membranes being used for carbon dioxide separation from syngas (Fig. 2).[3] Polymeric membranes have been at demonstration stage for carbon dioxide removal from natural gas for some time. Inorganic membranes however, generally of higher cost, remain at lab-scale pilot level for *e.g.* hydrogen separation using palladium membranes and at proof-of-concept stage for dense inorganic membranes, such as supported molten-salt membranes (Fig. 2).

1.2 Membrane Separation of Carbon Dioxide

Ideally, membranes selectively separate targeted component(s) of a mixture with fast permeant transport through the membrane. In gas separation, the driving force for

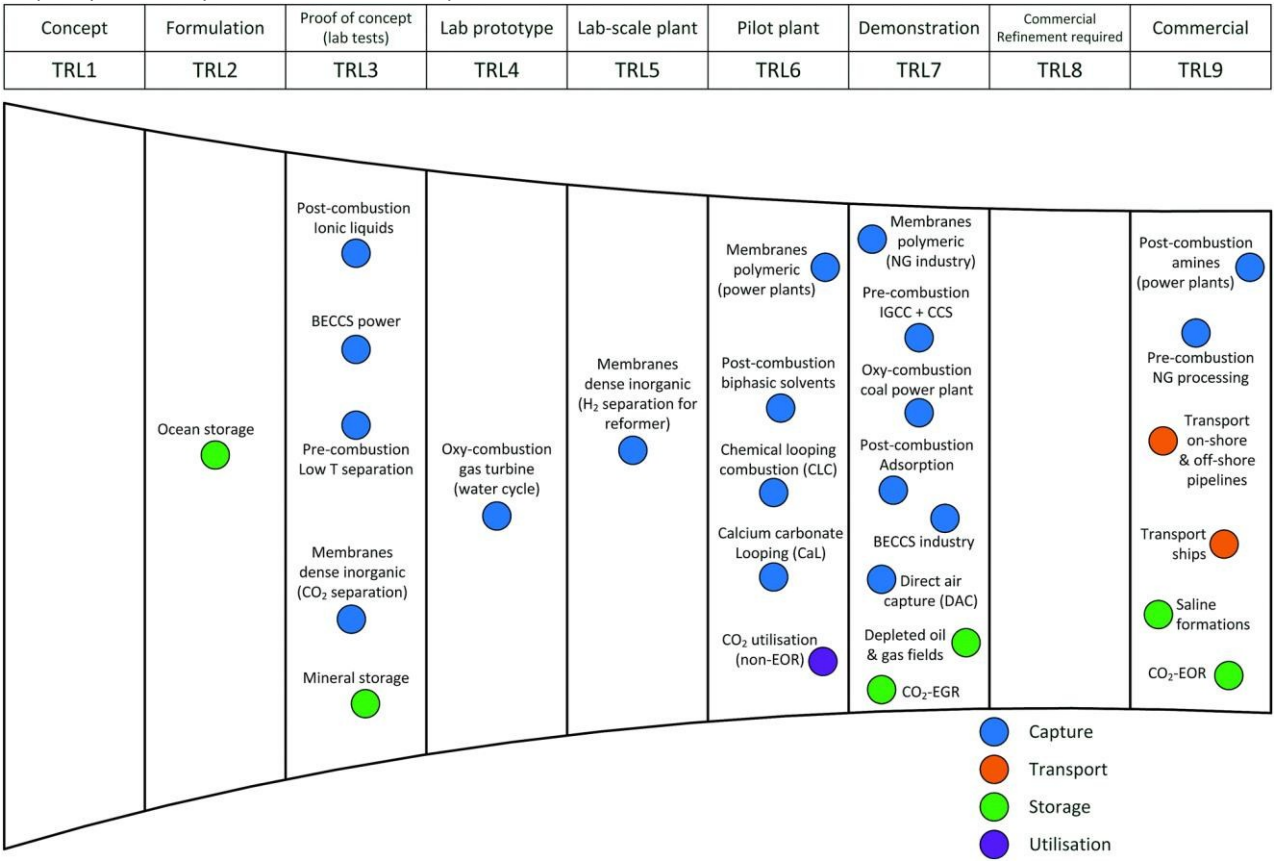

Fig. 2 – Technology readiness levels (TRL) of carbon capture, storage and utilisation technologies. Note that polymeric membranes have reached TRL7 with dense inorganic membranes for carbon dioxide separation at TRL3. Adapted from reference 3.

View Article Online
DOI: 10.1039/C9TA01979K

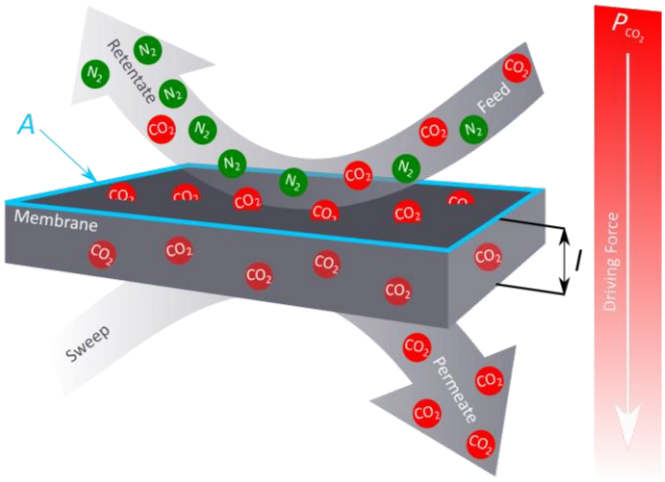

Fig. 3 – Membrane separation of carbon dioxide. A partial pressure difference across the membrane drives carbon dioxide permeation, with the membrane providing selectivity. The driving force, membrane area (*A*) and thickness (*l*) are used to calculate membrane performance metrics such as flux, permeability and permeance.

transport typically comes from a partial pressure difference between the feed and permeate sides of the membrane, ($p_f - p_p$) (Fig. 3). For permeant transfer from feed to permeate stream, it follows that $p_f > p_p$.

Membrane flux (j_i) is the volume, or number of moles, of permeant, *i*, transported per unit membrane area per unit time. Permeability is the flux normalised for the membrane thickness (*l*) and driving force (Equation 1), while permeance is normalised only for the driving force (Equation 2). Selectivity is the ratio of permeabilities (or permeances) for two or more components in the original mixture.

$$\text{Permeability} = j_i \frac{l}{p_f - p_p} \qquad (1)$$

$$\text{Permeance} = \frac{j_i}{p_f - p_p} \qquad (2)$$

Permeability and permeance at a given temperature can be used to compare membrane performance, as they are intrinsic properties of the membrane.[i] The permeability of a membrane is an intrinsic property of the membrane material, typically polymeric, ceramic or metallic and the membrane structure, dense or porous. In polymeric membranes (or any membrane that relies on solution-diffusion), permeability is related to the product of the solubility coefficient and diffusion coefficient of the permeant in the membrane material (Equation 3).

$$\text{Permeability} = S_i \times D_i \qquad (3)$$

In traditional dense polymeric membranes for gas separation, permeability differences arise due to differences in permeant diffusivities and solubilities. As free-pore volume is introduced to enhance diffusion rates, pathways with lower resistance are opened and selectivity is compromised. For polymeric membranes, this relationship is characterised by the Robeson upper bound (Fig. 4).[16]

To overcome the upper bound, a way to increase permeability without sacrificing selectivity must be found. Facilitated-transport membranes can achieve this using carrier-mediated transport processes. Carriers can be introduced into porous membranes through the addition of functional groups with high affinity for the permeant (fixed-carrier) or, in supported-liquid membranes, through the use of liquids with suitable reactivity towards the permeant (mobile-carrier). The latter approach, depending on liquid selection, could in theory offer high permeability and infinite selectivity; the membrane can be considered "pseudo-dense", with the liquid "closing" the pathways of lower resistance, whilst offering a selective pathway with high diffusivity.

Permeabilities of $10^3 - 10^4$ Ba ($10^{-13} - 10^{-12}$ mol m^{-1} s^{-1} Pa^{-1}) with carbon dioxide/nitrogen selectivity of 50 – 100 are required for economically feasible membrane separation of carbon dioxide.[17] Generally, polymeric membranes do not meet these targets, best represented by the current upper bound (Fig. 4). Notable exceptions include mixed-matrix membranes,[18] polymers of intrinsic microporosity and thermally rearranged polymers.[19] Zeolite membranes offer high selectivity but moderate permeability, whereas MOF membranes typically increase permeability at the expense of selectivity, compared to pure polymers.[18] Supported molten-salt membranes, where the salt is a molten carbonate, have carbon dioxide permeabilities of $10^{-12} - 10^{-10}$ mol m^{-1} s^{-1} Pa^{-1} at high temperature (>600°C). Hence, their intrinsic properties suggest that they offer promise for carbon dioxide separation. Furthermore, supported molten-salt membranes can be operated in the temperature range of ~400 – 1000°C, unlike polymeric membranes which are largely confined to lower temperature application. This operating range could allow exciting applications such as *in-situ* carbon dioxide removal from the high-temperature water-gas-shift

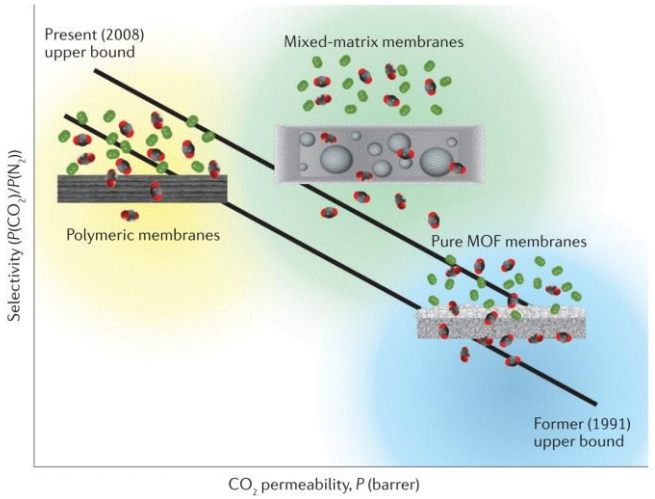

Fig. 4 – Carbon dioxide selectivity vs carbon dioxide permeability for polymeric, mixed-matrix (*i.e.* MOFs within polymeric) and pure MOF membranes, compared to the 1991 and 2008 upper bounds. Adapted from reference 18.

[i] This is only possible if the active membrane area and thickness are well-defined, which is often difficult to do with high precision.

View Article Online
DOI: 10.1039/C9TA00979K

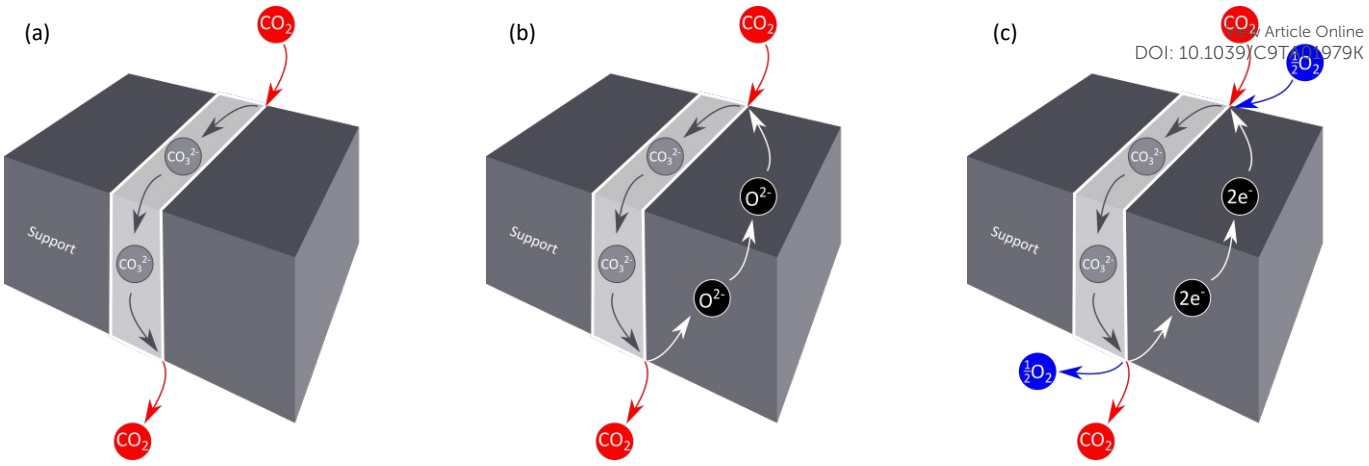

Fig. 5 – Proposed mechanisms for supported molten-carbonate membranes using (a) an electrically insulating support where carbon dioxide transport is restricted to the molten salt alone (species within the molten salt can react with carbon dioxide to produce "carbonate-like" carrier species, shown here as carbon dioxide for simplicity, with the required counter-current transport of a charge compensating species not shown), (b) an oxygen-ion-conducting support for pure carbon dioxide permeation with counter-current transport of O^{2-} in the support and CO_3^{2-} in the molten salt and, (c) an electron-conducting support for carbon dioxide and oxygen permeation with counter-current transport of e^- in the support and CO_3^{2-} in the molten salt.

reaction and carbon dioxide separation from hot flue gas streams.

2. Materials Selection for Supported Molten-Salt Membranes

A supported molten-salt membrane (also referred to as a dual-phase molten-salt membrane) comprises a porous inorganic support, with a molten salt infiltrated into the pore space (for carbon dioxide separation, the salts investigated so far have been molten carbonates). The support's physical properties impact separation performance *e.g.* thickness, acidity/wettability, pore volume and size, and tortuosity. In certain scenarios, ionic or electronic transport of species within the support may also contribute to permeation (Fig. 5). With an electrically insulating support, carbon dioxide permeation may be facilitated by "carbonate-like" species through reaction between carbon dioxide and ions in melt, *e.g.* oxide ($CO_2 + O^{2-} = CO_3^{2-}$) or carbonate ($CO_2 + CO_3^{2-} = C_2O_5^{2-}$) (Fig. 5a). With an oxygen-ion conducting support, reaction can occur with oxygen ions supplied from the support ($CO_2 + O^{2-} = CO_3^{2-}$) (Fig. 5b). Electron-conducting supports require oxygen in the gas phase with carbon dioxide ($CO_2 + ½O_2 + 2e^- = CO_3^{2-}$) (Fig. 5c). As will be elaborated upon later, a number of species responsible for transport have been proposed.

Methods to modify and control the physico-chemical properties of the inorganic supports are required to tailor the efficiency of separation. The molten salt component consists of anions and cations; their transport therefore opens opportunities to influence mechanism through manipulation of counter-ion or charge transport (Fig. 5). Molten carbonate salts also possess flexible physical properties as compared to other liquids in the wider class of supported-liquid membranes, *e.g.* tuneable wettability and vapour pressure in a large temperature range. However, they are also chemically reactive and corrosive, and impose strict requirements on the support materials. Below, we discuss the molten carbonate salt and inorganic support materials chemistry, in the context of preparation and operation of supported molten-salt membranes for high-temperature carbon dioxide permeation.

2.1 Molten Carbonate Properties

Most often, the molten carbonate salt used for supported molten-salt membranes is the $Li_2CO_3 – Na_2CO_3 – K_2CO_3$ (43.5 – 31.5 – 25 mol%) ternary eutectic carbonate mixture. One would assume that this is due to the low melting point (Fig. 6),[20] although pure Li_2CO_3 and binary mixtures have been investigated.[21] Here we focus on the properties of the ternary eutectic carbonate mixture. Entirely different melts (*e.g.* nitrate) may be used to fabricate selective supported molten-salt membranes, as we detail in Section 3.

Salt Melting & Decomposition

The nature of the electrostatic interactions leading to structural order in molten salts provides a theoretical basis for many properties of importance for supported molten-salt membranes. Coulombic interactions dominate in molten salts, while hydrogen bonding dominates in other liquids used in supported-liquid membranes *e.g.* ionic liquids,[22] or aqueous amines. The temperature where molten salt membranes are of promise is around the onset of common ionic liquid decomposition,[23] and obviously far above that of aqueous solutions. As an example, the ternary eutectic carbonate mixture melts just below 400°C (Fig. 6),[24] with little gas atmosphere dependent variation[25]. The relative strength of the

Salt system	Melting point (°C)
Li_2CO_3	723
Na_2CO_3	854
K_2CO_3	891
Li_2CO_3– Na_2CO_3 (52–48 mol %)	501
Li_2CO_3– K_2CO_3 (62–38 mol %)	498
Na_2CO_3– K_2CO_3 (56–44 mol %)	710
Li_2CO_3– Na_2CO_3– K_2CO_3 (43.5–31.5–25 mol %)	397
K_2CO_3–$MgCO_3$ (57–43 mol %)	460

Fig. 6 – Melting points of a range of carbonates and their mixtures. Adapted from reference 20.

Coulombic interaction in molten carbonate, permits operation at high temperature in the presence of carbon dioxide; in pure carbon dioxide the ternary eutectic carbonate mixture is stable to 1000°C.[25ii] Under an inert atmosphere the same melt completely decomposes.[26] Such strong Coulombic interactions provide low vapour pressures as exemplified with the independently measured pCO_2 from carbonate decomposition ($CO_3^{2-} = O^{2-} + CO_2$) of 5.3 x 10^2 and 6.7 x 10^2 Pa at 700°C for the ternary melt.[27,28] Hence, the membranes may be operated under a wide range of operational conditions, including in the presence of low pressures of carbon dioxide.

Viscosity & Density

Thermo-physical properties of the melt vary depending on the temperature and atmosphere. For instance, viscosity of the ternary melt decreases from 40 mPa·s at 400°C to 8 mPa·s at 650°C, with unary and binary molten carbonates on the same order of magnitude.[29,30] At high temperature (*i.e.* ~650°C), the viscosity of molten carbonates is therefore of the same order of magnitude as water at 20°C (1.002 mPa·s),[31] and at least one order of magnitude lower than typical ionic liquids.[32] Provided that suitable wetting of the molten salt on the support is achieved, this low viscosity facilitates the infiltration of the liquid melt into a range of pore structures and sizes. In the case of ionic liquids, often solvent blending or the application of a vacuum is used, whereas melting of carbonate powders in contact with porous supports enables infiltration of supported molten-salt membrane supports. Melt density/molar volume can be used to estimate the loading into porous supports. At 650°C, density of the ternary melt is ~2000 kg m^{-3},[26,33] again comparable with that of water at 20°C (~1000 kg m^{-3}),[34] decreasing slightly with increasing temperature.[33] Molar volume therefore increases with temperature, with composition dependent molar volume approximated by component additivity.[33]

Surface Tension & Wettability

Surface tension of the ternary eutectic carbonate mixture is around 240 mJ m^{-2} at 400°C decreasing to 220 mJ m^{-2} at 650°C (water at 20°C is ~73 mJ m^{-2}).[33,35] These values are significantly lower than the surface energy of potential ceramic supports in the same temperature range (*e.g.* 1.84 J m^{-2} for alumina and 1.53 J m^{-2} for 8% yttria-stabilised zirconia (YSZ) at 650°C).[36,37] This difference will lead to very low values of contact angles (θ) between the molten carbonates and the ceramics, enhancing gas-melt contact area. Interfacial tension depends on the surface energy of the membrane support material in contact with the molten carbonate. For ceramic supported molten-salt membranes, multiple ceramic supports show very good wettability by molten carbonate (Fig. 7). Such highly-wetting behaviour increases the adhesion between the substrate and molten carbonate, facilitates infiltration and, depending on the pore size, encourages carbonate retention when exposed to a pressure difference, which may be important for specific applications. The maximum pressure difference a supported molten-salt membrane can tolerate can be estimated by the

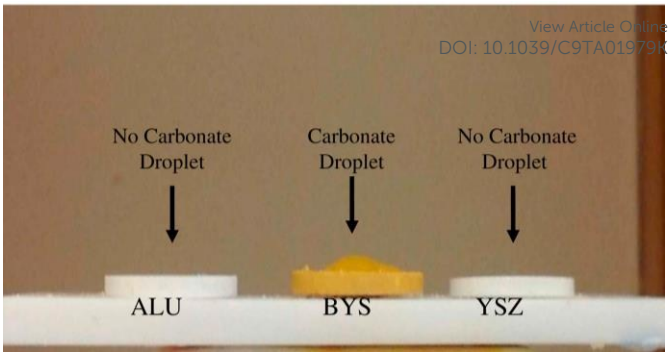

Fig. 7 – Wettability of lithium, sodium, potassium ternary eutectic carbonate mixture on alumina, BYS and YSZ ceramic membrane support materials upon melting at 550 °C. Adapted from reference 38.

Laplace equation (Equation 4), assuming a straight pore where, r, θ and γ are the pore radius, the contact angle of the molten salt, and the surface tension, respectively, and P' and P'' are the total pressure in the feed and permeate side, respectively.

$$\nabla P = P' - P'' = \frac{2\gamma cos\theta}{r} \qquad (4)$$

This relationship imposes several restrictions for the preparation and operation of supported molten-salt membranes. Infiltration of the molten salt in supports of average pore radius <1 µm will require larger differential pressure compared to supports of average pore radius >10 µm (Fig. 8). Furthermore, an appropriate pore structure is required,

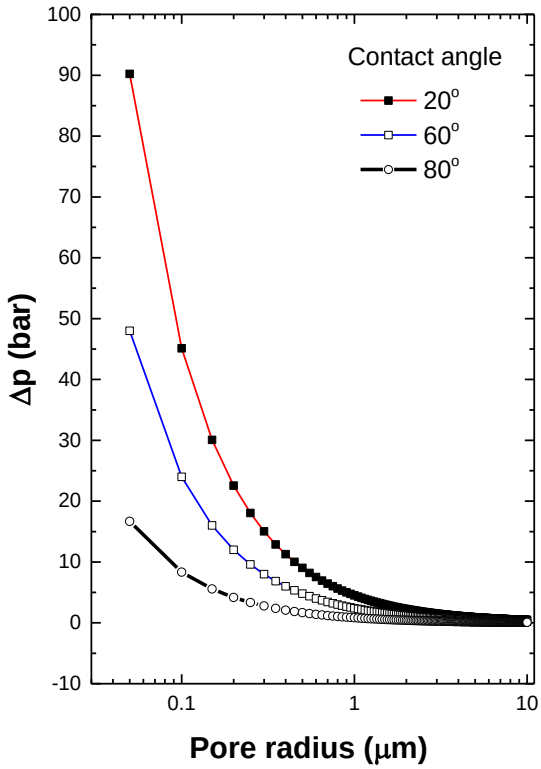

Fig. 8 – Examples of pressure differences tolerated by supported molten-salt membranes as a function of solid support pore size (calculated from the Young-Laplace equation for a given surface tension and three contact angles).

[ii] The authors did not state a pressure. Therefore, ambient pressure is assumed.

i.e. connected and with an exit so that occluded gases can escape. Applications where the membrane will have to operate with a high transmembrane pressure difference will tend to promote molten salt creep if the pore size of the support does not enable retention of the molten salt by capillary forces. It should also be noted that gas phase composition can change the molten salt contact angle. However, this phenomenon is poorly studied.

Tailoring the wettability of the molten salt towards the ceramic support has also been used to produce thinner membranes, *i.e.* to confine the molten salt to a defined layer, coated onto a non-wetting macroporous support which provides the overall mechanical stability of the membrane.[38]

Gas Solubility

It is important to define exactly what is meant by solubilities in molten salts, as they can be separated into physical and chemical (or reactive) solubilities.[39] A simple analogy would be the dissolution of carbon dioxide into water. Carbon dioxide first dissolves to form $CO_2(aq)$ with an equilibrium subsequently formed between $CO_2(aq)$ and H_2CO_3. Dissociation products include H^+, HCO_3^- and CO_3^{2-}. $CO_2(aq)$ is the physical solubility product with all other species chemical (or reactive) solubility products. Molten carbonates generally have low physical solubilities for gases, but high chemical solubilities (~50 times greater for carbon dioxide in molten carbonate).[27] Using water again as a comparison, this is quite different, as in water the physical solubility product $CO_2(aq)$ has orders of magnitude higher solubility than the chemical solubility products. A comprehensive summary of gas solubilities in molten salts has been provided by IUPAC, with hydrogen, oxygen, nitrogen, carbon monoxide and carbon dioxide solubilities given for a range of carbonate compositions.[40] Significant variation is apparent, attributed to the difficulty in distinguishing between physical and chemical solubility, and a lack of appropriate experimental techniques.[27] Briefly, solubility of nitrogen is purely physical due to the non-interacting nature of the inert gas; therefore low and comparable with the physical component of carbon monoxide solubility. Solubility determination for hydrogen is complicated due to the formation of carbon monoxide *via* the reverse water-gas-shift reaction with carbon dioxide.[40,41]

Carbon dioxide solubilities in molten carbonates are around two orders of magnitude higher than in nitrate or halide melts.[27,42,43] Due to variation in the literature, no reliable value can be extracted. As carbon dioxide chemical dissolution in molten carbonates is kinetically slow, solubility may appear to increase with temperature. Being a weak acid, a determining factor for carbon dioxide solubility is melt basicity.[39] Thus, lithium dominated melts offer the highest solubilities. Oxygen solubility is also a combination of physical and chemical components, overall, far lower than carbon dioxide but still dominated by chemical solubility.[44] Early investigations were plagued with uncertainty due to the lower solubility and complexity of formed species,[41] with recent titration methods providing more reliable data.[44,45] The point to be stressed in the current review, is that carbon dioxide solubility is very high, with oxygen solubility appreciable, inert gases negligible and others inconclusive. It should therefore be quite clear that reliable methods and an up-to-date authoritative and systematic study of solubility *vs* composition for a range of relevant gases in molten carbonates would be useful.

Speciation

Chemical solubility introduces speciation in molten carbonates, pertinent to both carbon dioxide and oxygen, where a large variety of carbonate and oxide species have been either identified experimentally or found to be theoretically stable in molten carbonate.[46]

As mentioned above, physical oxygen solubility is negligible, with chemical solubility products including superoxide (O_2^-), peroxide (O_2^{2-}) and peroxymonocarbonate (CO_4^{2-}). The CO_4^{2-} species has been proposed as responsible for oxygen transport within molten carbonate by DFT calculation (Fig. 9).[47] Oxygen

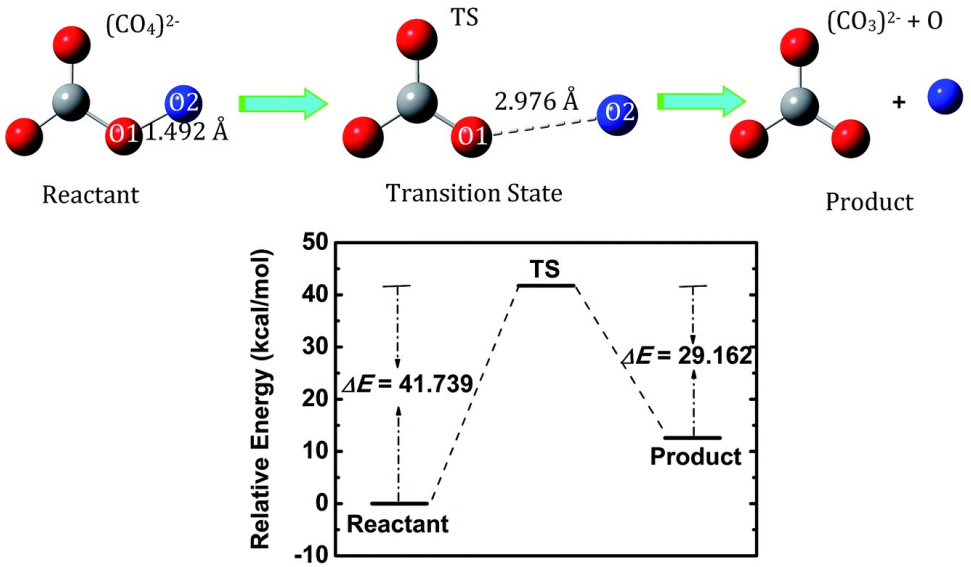

Fig. 9 – Structures of CO_4^{2-} related species, proposed as responsible for oxygen transport in molten carbonate. The relative energetics indicate that CO_3^{2-} could act as a mobile carrier for oxygen, in a facilitated-transport "cog-wheel" mechanism. With oxygen passed from carbonate to carbonate, CO_4^{2-} is seen as an oxygen carrier. Adapted from reference 47.

DOI: 10.1039/C9TA01979K

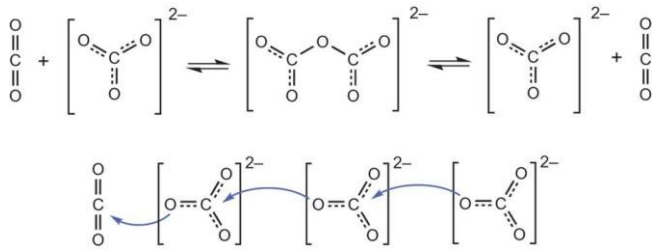

Fig. 10 – Oxo-Grotthuss mechanism for carbon dioxide transport in molten calcium carbonate. The $C_2O_5^{2-}$ species responsible for fast ionic transport of carbon dioxide is also attributed to the high carbon dioxide solubility in molten carbonate. Adapted from reference 50.

speciation is strongly influenced by melt basicity, with peroxides stabilised in strongly basic lithium or sodium dominated melts and superoxides prevalent in weakly basic/weakly acidic potassium dominated melts.[48,49] Adding foreign cations or nitrates offers a simple way to enhance oxygen solubility and increase the oxidising power of the melt further.[48] Two extremes in oxidising power can be considered: low pCO_2 and therefore high oxygen-ion activity and a basic melt, or, high pCO_2 and therefore low oxygen-ion activity and an acidic melt.

Reaction between carbon dioxide and carbonate to produce $C_2O_5^{2-}$ provides one route to the aforementioned high solubility ($CO_2 + CO_3^{2-} = C_2O_5^{2-}$),[42] yet unlike the oxide species above which form rapidly, equilibration between carbon dioxide and $C_2O_5^{2-}$ is a slow process.[27] However, the same $C_2O_5^{2-}$ species have been proposed to provide a fast transport pathway, by an oxo-Grotthuss mechanism (Fig. 10), in molten calcium carbonate (the diffusion coefficient is three times greater than that of CO_3^{2-}).[50] Indeed, $C_2O_5^{2-}$ has been spectroscopically identified and proposed as involved in the permeation of carbon dioxide in a supported molten-salt membrane.[51] From DFT calculations, it would appear that $C_2O_5^{2-}$ is stabilised by small cations, *e.g.* H^+ and Li^+,[52] although this is only reported in one study. More work should be done to better understand the $C_2O_5^{2-}$ species as it would appear to have many of the characteristics required for fast facilitated-transport and high solubility of carbon dioxide (Equation 3).

Release of carbon dioxide from CO_3^{2-} will produce dissolved oxide (O^{2-}) within the molten carbonate ($CO_3^{2-} = O^{2-} + CO_2$) and reaction between oxide and water can also produce hydroxide (OH^-) ions.[53] As the counter-current transport of a charge-compensating species is required for an appreciable carbon dioxide flux (Fig. 5), *i.e.* neutral carbon dioxide transport in molten carbonate is negligible compared to transport of ionic species, the addition of dissolved oxide in molten carbonate has been shown to enhance carbon dioxide flux through increasing the concentration and conductivity of dissolved oxide species.[54] Hydroxide ions have also been exploited as counter-current transport species. In such cases, either through introduction of water in the sweep gas,[55] or the partial replacement of molten carbonate by molten hydroxide,[56] significant flux enhancements were noted, as molten phase diffusivities were exploited, as well as or in place of, oxygen-ion transport in the solid support, respectively. Overall, a complex picture develops, and as has been pointed out previously,[57] far greater consideration should be given to this in the context of supported molten-salt membrane operation in the future.

Diffusion

Diffusion in the molten salt is of significant interest for supported molten-salt membranes, due to its importance in permeability (Equation 3) and the transport of species through the membrane. Diffusion in a large number of molten salts has been reviewed, with the data for molten carbonates indicating that diffusion coefficients are on the order of 10^{-9} m^2 s^{-1} for both cation and anion diffusion.[58] More recently, cation diffusion was proposed to be one order of magnitude higher than CO_3^{2-} diffusion in carbonate melts.[59] Computational approaches tend to underestimate diffusion coefficients compared to experiments,[59,60] however, unlike solubility, diffusion coefficients seem to generally agree, albeit from a small number of studies. The difficulty of course, is in understanding which species, and their associated diffusivities, are important for permeant transport.

2.2 Membrane Support Properties

Supports for molten-salt membranes are inorganic due to the requirement of high-temperature stability. Initially, metals were used as supports, with functional ceramics investigated later. Here we restrict ourselves to a discussion of the requirements for supports, and achievements to date in terms of tailoring their physico-chemical properties to meet these, specifically the materials used previously in supported molten-salt membranes. Excellent ionic and/or electronic conductivities (for conducting supports), chemical stability at high temperatures and good wettability by molten carbonate are key requirements for developing high flux membranes.[61,62] Additionally, support microstructural control has been pursued to confine the melt in the inorganic support, and enhance interfacial pathways. This includes pore volume, pore size and tortuosity.[63]

Electrically Insulating Supports

Alumina is an electrically insulating metal oxide that has been applied as a support for molten carbonates,[21] and more widely as a support for adsorbents and catalysis, because of its high-temperature chemical and physical stability. Due to the excellent wetting of molten carbonate on alumina, it has also been used to modify the surface of supported molten-salt membranes to improve molten salt retention.[64–66] In the presence of molten carbonate the alumina layer converts to lithium aluminate, which further improves the wettability by the molten carbonates.[67]

Oxygen-Ion Conducting Supports

Oxygen-ion conducting materials with a fluorite structure (Fig. 11), *e.g.* rare-earth-doped ceria and YSZ, have been extensively investigated as supports for molten-salt membranes. An effective approach to enhance the oxygen-ion conductivity (here in an effort to improve permeation, (Fig. 5b)) is to increase the oxygen vacancy concentration by doping bivalent and trivalent cations into the parent structure. For instance, scandium oxide-doped zirconia has higher oxygen-ion conductivity than YSZ and calcium oxide-doped zirconia, due to

View Article Online
DOI: 10.1039/C9TA01979K

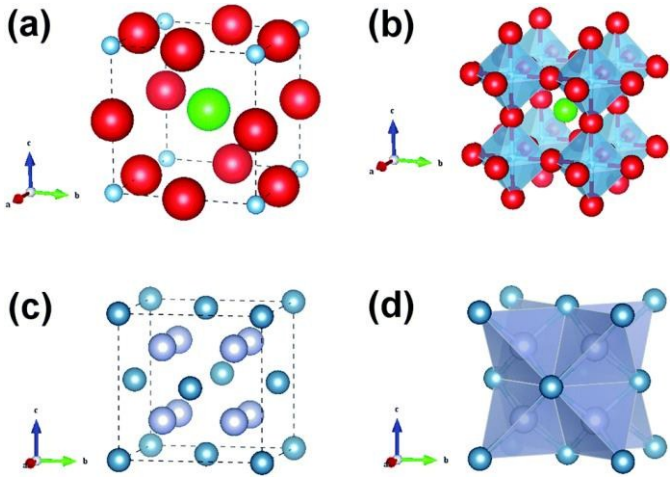

Fig. 11 – Structure and packing arrangement for (a, b) perovskite ABO_3 (A – green, B – blue, O – red) and, (c, d) fluorite AO_2 (A – blue, O – grey). Adapted from reference 70.

its lower dopant solution energy for forming the solid solution, based on atomistic simulation.[68]

Rare-earth-doped ceria has high oxygen-ion diffusivity and conductivity (~10^{-2} S cm^{-1}). The incorporation of a trivalent dopant with a large ionic radius introduces lattice strain, decreasing the activation energy for oxygen-ion migration, overall enhancing oxygen-ion diffusivity.[69] Under a reducing atmosphere, or low oxygen partial pressure, Ce^{4+} can be reduced to Ce^{3+}, which creates oxygen vacancies and enhances electronic conductivity.[70] Gd^{3+} and Sm^{3+} doped ceria exhibit the highest oxygen-ion conductivity (Fig. 12),[71] compared with

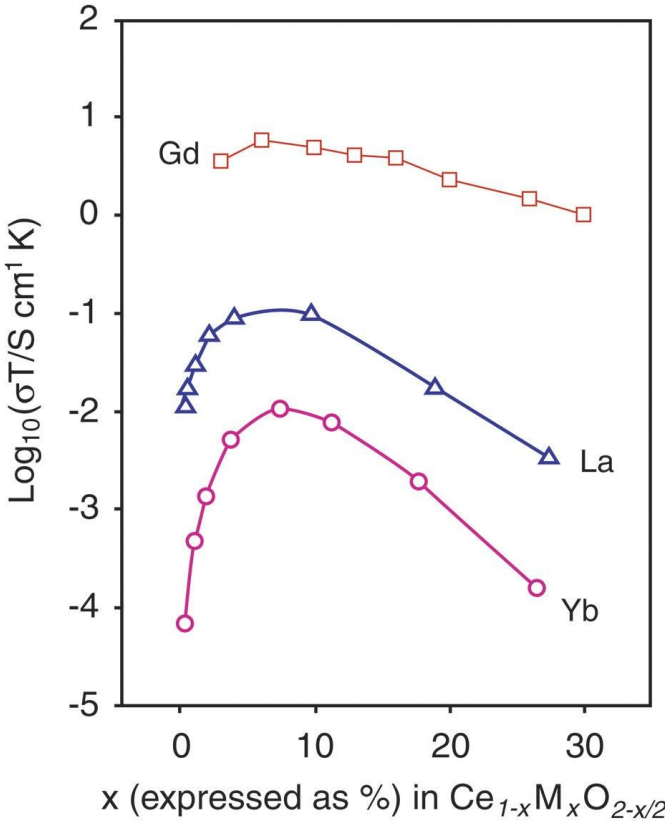

Fig. 12 – Isothermal conductivity of ceria solid solutions. Doping with *i.e.* Gd^{3+} increases oxygen-ion conductivity of ceria. Adapted from reference 71.

other rare-earth-doped ceria.[72] In Sm_2O_3-doped ceria/sodium carbonate nanocomposite, both proton and oxygen-ion conductivity have been reported.[73]

Cubic fluorite δ-Bi_2O_3 is an excellent oxygen ionic conductor with a very high oxygen ion conductivity of 2.3 S cm^{-1} at 800 °C.[74] Doping δ-Bi_2O_3 with rare-earth cations (*e.g.* $Bi_{1.5}Y_{0.3}Sm_{0.2}O_3$ (BYS)) can stabilize the fluorite structure and result in an increase in oxygen ion conductivity at low temperatures.[75] The carbonate wettability of BYS is reported to be limited at elevated temperatures, hence requiring modification of pore and membrane surfaces.[38] For instance, the deposition of an alumina layer on the BYS membrane has been applied to enhance the surface wettability and infiltration of molten carbonate salts.[66]

Electron Conducting Supports

Initial attempts to create supported molten-salt membranes with electronically conductive metal substrates used stainless steel (~10^4 S cm^{-1} at 20°C), infiltrated with a lithium, sodium, potassium ternary eutectic carbonate mixture.[76] Interfacial steel-carbonate reactions at temperatures above 650 °C, leads to the formation of Li-Fe-O phases on the surface of the support. As the electronic conductivity of these oxides phases is very low, the electron transport pathway through the support is lost and the performance of the membrane is severely affected.[77] Silver shows the highest electronic conductivity among all metals (~10^5 S cm^{-1} at 20°C) and, reasonable corrosion resistance in molten carbonates.[78] Therefore metallic silver has been used as a support for supported molten-salt membranes.[79] Pure silver membranes exhibit much less interfacial reaction compared to steel, but again the long term performance of the membrane at temperatures above 650 °C is poor. This is due to limited wettability of silver by the carbonates,[80] and silver sintering, causing loss of the molten carbonate phase from the silver support as the porosity is reduced and pores enlarge.[79,81] The aforementioned alumina surface modification or,[64] zirconia atomic layer deposition (ALD),[82] improved both high-temperature stability and long-term operation potential by improving wettability and limiting sintering.

Mixed Ion-Electron Conducting Supports

Electron conducting supports exhibit good permeation performance but, besides interfacial reactions limiting long-term stability, the lack of oxygen-ion conductivity demands the presence of oxygen in the feed-gas to form carbonate ions for transport through the molten salt (*i.e.* $CO_2 + ½O_2 + 2e^- = CO_3^{2-}$). In turn, oxygen is present in the permeate stream, obviously no longer providing a purely carbon dioxide selective membrane. Metal supports can be replaced by materials with mixed electronic and ionic conductivity (MIEC). In this case, oxygen is no longer required in the feed gas stream for the membrane to operate.

Most MIEC materials used as supports for molten salts are perovskite-type structures (Fig. 11), ABO_3, where A is a rare earth element and B is a transition metal.[83] Among the perovskites, $(La, Sr)(Co, Fe)O_{3-\delta}$ (LSCF) is known to exhibit high mixed ionic and electronic conductivity at temperatures above 700 °C.[84,85] Typical electronic conductivities for LSCF are ~10^2 S

View Article Online
DOI: 10.1039/C9TA01070H

cm^{-1} with oxygen-ion conductivities ~10^{-1} S cm^{-1}. The first supported molten-salt MIEC membrane reported used an LSCF support, but showed decreasing performance with time,[86] due to the formation of cobalt oxide and strontium carbonate at the gas-support interface from reaction with carbon dioxide.[62] These phases decreased the overall conductivity of the support, negatively impacting permeation with time. Addition of oxygen in the feed gas has been shown to significantly improve the long term stability of the membrane,[62,87] but oxygen will then also permeate through the membrane.

Different perovskite structures and perovskite-fluorite mixtures have been tested in order to improve thermochemical stability. $La_{0.85}Ce_{0.1}Ga_{0.3}Fe_{0.65}Al_{0.05}O_{3-\delta}$ (LCGFA) membranes have shown good chemical and thermal stability, during carbon dioxide permeation under a range of gas atmospheres at high temperatures.[88] $SrFe_{0.8}Nb_{0.2}O_{3-\delta}$ membranes tested for 200 hours by Jiang *et al*. also showed improved long term chemical stability as well as thermal cycling stability under carbon dioxide rich atmospheres.[89] Recently a fluorite $Ce_{0.85}Sm_{0.15}O_2$ (SDC) and perovskite $Sm_{0.6}Sr_{0.4}Al_{0.3}Fe_{0.7}O_3$ composite was reported to have good thermochemical stability at 800 - 950 °C as an oxygen-ion conducting oxygen separation membrane, with a carbon dioxide sweep-gas. Subsequently, SDC-$Sm_{0.6}Sr_{0.4}Al_{0.3}Fe_{0.7}O_3$ was used to prepare a supported molten-salt membrane.[90] Au-Pd deposition on the feed side of the same membrane was proposed to increase the electron density and therefore CO_3^{2-} formation, thus enhancing the carbon dioxide permeance.[91]

2.3 Support Microstructure and Macroscopic Geometry

The physical properties of the support in a supported molten-salt membrane define characteristics such as thickness, porosity, tortuosity, triple-phase-boundary length and the overall geometry of the membrane. The literature on supported molten-salt membranes is dominated by pellets prepared by isostatic compression and tape-casting approaches,[21,88] due to the ease of preparation and suitability for laboratory-scale experiments. More recently, advanced support geometries with hierarchical microstructures promoting thinner membranes likely to improve membrane performance have been used for supported molten-salt membranes. Examples include hollow fibres, fabricated by phase inversion and sintering techniques,[92] and asymmetric membranes (a thin separation layer on a mechanically robust support), prepared using phase inversion, tape-,[93] or centrifugal-casting,[94] and extrusion and slip-casting. Generally, a thin support (or, more specifically, a small active membrane thickness) with high porosity of low-tortuosity and with a geometry that can be assembled into robust membrane modules is desired.

Support Thickness

As the support retains the molten carbonate, its thickness coarsely defines the length scale for bulk diffusion through the membrane during permeation. Carbon dioxide permeance (Equation 2) increases with decreasing thickness in both $La_{0.6}Sr_{0.4}Fe_{0.2}O_{3-\delta}$ (LSF) and YSZ supported molten-salt membranes.[38,86] Effective activation energies also increased slightly with decreasing thickness, indicating that surface reactions (with higher activation energies than diffusion) become rate-limiting.[iii]

Generally, there is significant scope to improve permeance in supported molten-salt membranes (typically ~mm thickness) and suitable preparation methods should be developed for reducing the thickness of ceramic membrane supports further.

Porosity Control - Ceramics

The pore structure of supports, including pore volume, pore size, pore connectivity and tortuosity, influences carbon dioxide permeation because of its impact on particle interconnectivity, and the total conductivity of the support and carbonate.[63] Furthermore, porosity at the surface of the support coarsely defines the liquid-gas interfacial area and the triple-phase-boundary lengths at the feed and permeate sides of the membrane. Most commonly, sacrificial materials are used as pore formers, which are later removed and/or modified during the fabrication of the support, *e.g.* by burnout (organic removal), reduction (oxygen removal), and acid etching. The final porosity of the support can be controlled by the amount of the sacrificial material used, as well as its particle shape and size and the firing profile.[95,96]

An example of a recently proposed manufacturing route for the formation of porous ceramic supports with a uniform 3D network was described by Zhang *et al*.[97,98] A modified Pechini method is used to produce powders consisting of the precursors of the desired support materials mixed with precursors of a metal oxide that will be used as the sacrificial phase. The resultant mixed powder is pressed into a pellet, which is later fired under a reducing atmosphere in order to reduce the sacrificial phase to its metallic phase. Finally, the metallic phase is removed by acid etching to provide a unimodal distribution of connected pores of sub-micron scale (size depending on the support).[97,98]

Porosity Control - Metals

Porous metal membrane supports have been prepared by a dealloying method, where an alloy is etched by an aqueous acid solution to leave behind a porous scaffold of the desired metal. Silver supported molten-salt membranes with a pore size of 1-5 µm and 10 µm have been reported, using 50 at% Ag – 50 at% Al and 50 at% Ag - 50 at% Zn alloys, by chemical or electrochemical dealloying.[99,100] The advantage of this method is the formation of a well-connected porous network with uniform microstructure. The pore size and total porosity can be simply controlled by adjusting the dealloying time (Fig. 13). In the case of 50 at% Ag – 50 at% Al, α-Al dissolves faster than Ag_2Al, and as the alloy is far richer in α-Al, initially a network with pore sizes in the range of single to tens of µm is formed (Fig. 13c).[100] Subsequently, a sub-micron pore network derived from the Ag_2Al regions is formed (Fig. 13d). Sub-micron pores, and a high density of triple-phase-boundaries, contribute to an enhanced

[iii] It is common practice with supported molten-salt membranes to report effective activation energies for the permeation process, summing the individual surface reaction and diffusion steps.

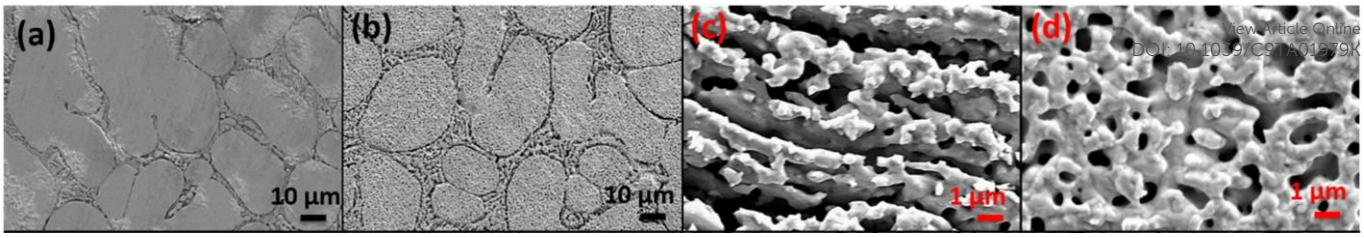

Fig. 13 – SEM images of (a) 50 at% Ag – 50 at% Al alloy, (b) porous Ag after 48 hours of chemical dealloying, (c) porous Ag from α-Al and, (d) porous Ag from Ag_2Al. Adapted from reference 100.

ability to retain molten carbonates and provide a high carbon dioxide flux.[99] A method using a sacrificial pore former has also been used for the preparation of porous silver.[101,102] The addition of 40 vol% carbon black in silver powder and firing at 650°C were used to create a porous network with pore size of ~10 µm,[101,102] while addition of 70 vol% microcrystalline methylcellulose and firing at the same temperature created a pore structure with a size of 15-20 µm.[64] The pore size and total porosity depends on the size of the pore former and its loading, its degree of de-agglomeration, casting parameters (which can further contribute to agglomeration and/or isolation of the pore former) and the thermal treatment.

Advanced Support Geometries

Recently, ceramic hollow fibres have been used as supports for molten salts as they offer high surface area/volume ratio and reduced membrane thickness.[103,104] Reasonable carbon dioxide fluxes have been reported for both YSZ and LSCF hollow-fibres.[105,106] Although the hollow fibre geometry is more amenable to scale-up than pellet membranes, *i.e.* relatively, hollow fibres possess an inherent modularity, the mechanical strength of the thin sintered ceramic fibres is presently fairly low. Multi-channel hollow fibres have been proposed to overcome this challenge, and recently prepared as supported molten-salt membranes. Multi-channel hollow fibre membranes comprising $SrFe_{0.8}Nb_{0.2}O_{3-\delta}$ and carbonates (Fig. 14), exhibited an increased thermomechanical strength and carbon dioxide flux as compared to single-channel hollow fibres.[89]

In asymmetric supported molten-salt membranes, the molten carbonate is confined to a thin carbonate-wetting ceramic layer (Fig. 15), which is supported by a thicker non-wetting macroporous layer ensuring mechanical strength. This has the effect of reducing the diffusion length for ionic transport in an ion-conducting support or in the confined salt. Pellet membranes with a non-wetting support and a 150 µm SDC or 10 µm YSZ layer exhibit higher carbon dioxide permeances than the equivalent symmetric membranes of greater thickness.[38,107] The same systems have been prepared as asymmetric tubular membranes, progressing towards a membrane geometry more suitable for scale-up.[94,108]

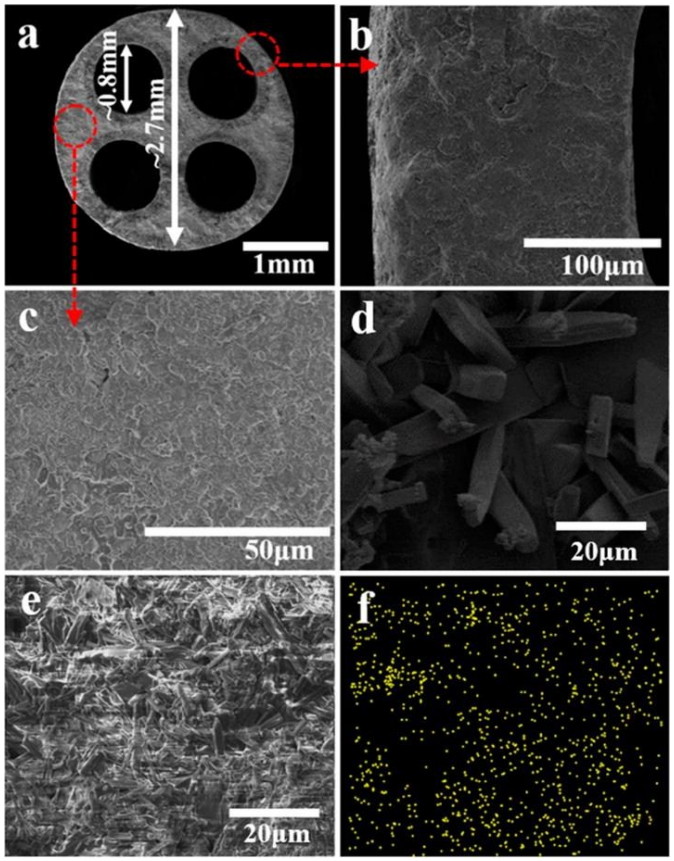

Fig. 14 – SEM images of a carbonate loaded multi-channel $SrFe_{0.8}Nb_{0.2}O_{3-\delta}$ hollow fibre supported molten-salt membrane. Multi-channel hollow fibres offer high surface to volume ratios and, relative to single-channel hollow fibres, increased mechanical strength. (a) Cross-section, (b) outer wall, (c) high magnification of cross section, (d) inner surface, (e) outer surface and, (f) EDX of potassium in cross-section. Adapted from reference 89.

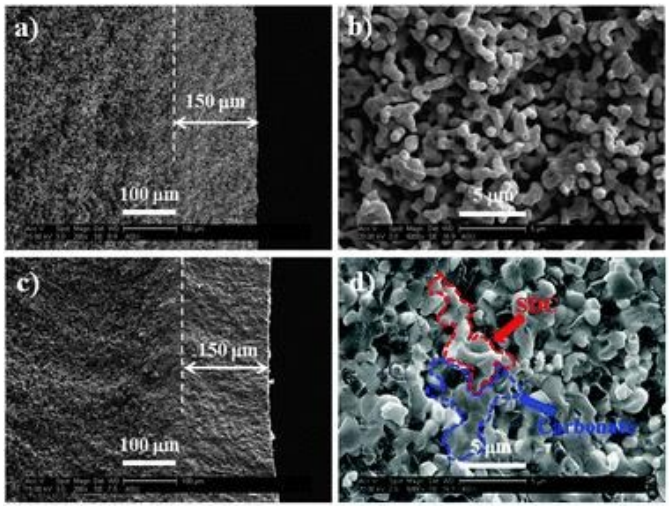

Fig. 15 – SEM images of an asymmetric supported molten-salt membrane consisting of a 150 µm $Ce_{0.8}Sm_{0.2}O_{2-\delta}$ layer on a $Ce_{0.8}Sm_{0.2}O_{2-\delta}$ - $Bi_{1.5}Y_{0.3}Sm_{0.2}O_{3-\delta}$ support. (a) Cross-section and, (b) porous $Ce_{0.8}Sm_{0.2}O_{2-\delta}$ layer before carbonate infiltration. (c) Cross-section and, (d) porous $Ce_{0.8}Sm_{0.2}O_{2-\delta}$ layer after carbonate infiltration. Adapted from reference 94.

View Article Online
DOI: 10.1039/C9TA01979K

3. Supported Molten-Salt Membranes in Operation

Supported molten-salt membranes for carbon dioxide permeation can be broadly distinguished on the basis of the support phases introduced above, and their associated proposed permeation mechanisms: inert support (*e.g.* alumina), oxygen-ion-conducting support (*e.g.* ceria) to produce a mixed oxide-ion and carbonate-ion transport membrane and; electron-conducting support (*e.g.* stainless-steel) to produce a mixed electron and carbonate ion transport membrane. Here, we discuss reported permeation mechanisms and the associated permeation data for a range of supported molten-salt membranes. This is focussed on carbon dioxide permeation, with a small number of examples for alternative separations using supported non-carbonate molten salts. We make comment on the long-term stability of supported molten-salt membranes. Finally, we provide examples of supported molten-salt membranes applied in chemical reactions, and of supported molten-salt adsorbents, an entirely different geometry of supported molten-salt, but with application in carbon dioxide separation. The performance of a representative selection of the membranes discussed in subsequent sections are presented in Fig. 16. The reader is also referred to a number of supported molten-salt membrane articles that provide flux comparison tables for more focussed classes of supports.[57,89,90,106]

3.1 Carbon Dioxide Permeation

Molten carbonate supported in an oxygen-ion-conducting oxide, leads to pure carbon dioxide permeation [66,109] (Fig. 5b). When supported in an electron-conducting host, the co-permeation of carbon dioxide and oxygen is observed (Fig. 5c).[76,110] Initially we assume that bulk conductivities are rate determining. Thus, in the case of an oxygen-ion-conducting support for the carbonate phase the flux of carbon dioxide through the membrane can be described by:

$$j_{CO_2} = \frac{RT}{4F^2} \frac{\frac{\varepsilon\sigma_{CO_3}(1-\varepsilon)\sigma_O}{\tau_{CO_3} \quad \tau_O}}{\frac{\varepsilon\sigma_{CO_3}}{\tau_{CO_3}} + \frac{(1-\varepsilon)\sigma_O}{\tau_O}} \frac{d \ln P_{CO_2}}{dx} \qquad (5)$$

where σ_{CO3} is the effective conductivity of the carbonate ion, σ_O is the effective conductivity of the oxygen ion, ε is the membrane porosity and τ_{CO3} and τ_O are the tortuosities of the two phases. In the case of an electron-conducting support for the carbonate phase we must also modify the driving force to include the contribution from the difference in oxygen partial pressure across the membrane because of the co-permeation of carbon dioxide and oxygen. Here, σ_e is the effective electronic conductivity:

$$j_{CO_2} = \frac{RT}{4F^2} \frac{\frac{\varepsilon\sigma_{CO_3}(1-\varepsilon)\sigma_e}{\tau_{CO_3} \quad \tau_e}}{\frac{\varepsilon\sigma_{CO_3}}{\tau_{CO_3}} + \frac{(1-\varepsilon)\sigma_e}{\tau_e}} \frac{d\left(\ln P_{CO_2} + \frac{1}{2}\ln P_{O_2}\right)}{dx} \qquad (6)$$

In Equation 6, we see that it may be possible to reverse the direction of carbon dioxide permeation by using an oxygen partial pressure gradient of opposite sign that is greater than double the carbon dioxide partial pressure gradient. Such carbon dioxide permeation has been demonstrated, classified as being 'uphill'.[110]

In the absence of bulk control, the permeation rate (for sufficiently thin membranes) will be controlled by surface processes. The limiting rate could be controlled by carbon dioxide uptake on the feed side or carbon dioxide release at the permeate side. It is likely that the rate expression will be of a power-law kind dependent upon carbon dioxide partial pressure in the case of an oxygen-ion conducting support and both the partial pressure of carbon dioxide and oxygen in the case of an electron-conducting support. Furthermore, we note that the length of the three-phase-boundary between the carbonate phase, the electronic or oxygen-ion conducting phase and the gas phase is likely to influence the kinetics. It is also worth noting that at very high permeation rates the rate could be limited by mass transfer consideration in the gas phase.

Electron Conducting Supports

In the pioneering work of Lin *et al*. a porous stainless steel support was used to house a ternary eutectic carbonate mixture.[76] Such a support should clearly be electronically conducting and should thus require the presence of oxygen with carbon dioxide for permeation (Fig. 5). Single gas permeation rates for carbon dioxide and inert (nitrogen) were indeed investigated and found to be low, however the single gas permeation rate of oxygen does not appear to have been evaluated. On the other hand, the permeance with a feed gas of carbon dioxide:oxygen of 2:1 was up to 2.5 x 10^{-8} mol s^{-1} m^{-2} Pa^{-1} at 650°C (Fig. 17). Under these conditions the separately-measured nitrogen permeation rate yielded a separation factor of carbon dioxide over nitrogen of 16. The authors used a simple ambipolar conductivity model to predict the combined carbon dioxide and oxygen flux. They found this flux to be lower than expected and suggested that this could at least in part be due to interfacial reactions resulting in the formation of an electronically insulating interfacial phase of $LiFeO_2$. As the

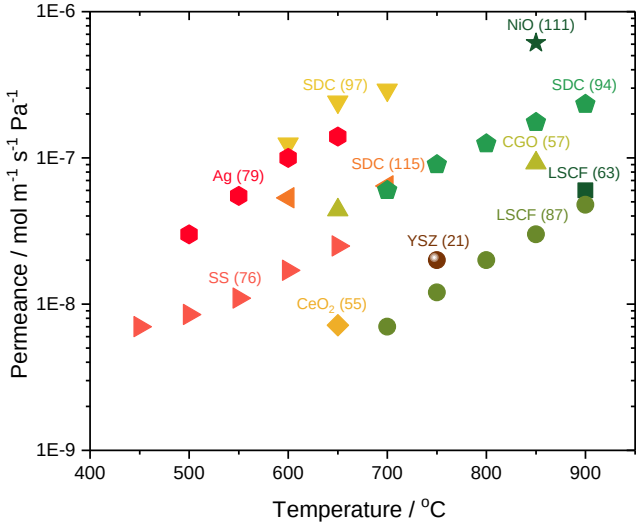

Fig. 16 - Examples of carbon dioxide permeance as a function of temperature for supported molten-salt membranes in the literature, where the salt is molten carbonate. Labels indicate support material and reference number. Readers are referred to the original publications for further detail.

permeation rate was determined by pressure change versus time there was unfortunately no indication of the ratio of carbon dioxide to oxygen found on the permeate side.

More recently other workers have exploited metallic supports less likely to undergo detrimental interfacial reactions, most commonly silver. In many cases, by looking at the permeate gas composition and specifically the ratio of the rate of carbon dioxide permeation to oxygen permeation, they have shown that conduction mechanisms may be more complicated than those envisaged in Fig. 5. Early work was performed by Huang *et al*. with a silver-supported binary lithium and potassium eutectic carbonate mixture.[79] The feed was a 1:1 carbon dioxide:oxygen ratio. The carbon dioxide permeance of the membrane reached 1.4 x 10^{-7} mol m^{-2} s^{-1} Pa_{CO2}^{-1} at 650°C, higher than that reported by Lin *et al*. (note that the driving force is different as a result of the different feed compositions in these two studies; in this class of membrane both carbon dioxide and oxygen partial pressure differences contribute to the driving force). In this particular case the permeate gas contained carbon dioxide and oxygen in the ratio of 2:1 as the simple model in Fig. 5 would suggest. While XRD did not indicate any phase changes during operation, silver grain growth did take place and this seems to have resulted in a loss of molten carbonate from the silver network. This molten carbonate loss from the membrane was used to explain a decrease in permeation rate between 20 and 80 hours of operation although it is unclear why such a loss would result in this effect. Further work explored the concept of depositing alumina on the silver surface to inhibit sintering and improve membrane stability,[64] and the use of membranes of different thicknesses to investigate the rate-determining step of the permeation process.[101]

ALD was also used to deposit both alumina,[47] and zirconia,[82] on silver, with SEM characterisation showing 20-25 nm layers. It is unclear why such layers do not impede permeation (which requires an electronically conducting support). It would be logical to worry about the composition of the alumina or zirconia layer (are there impurities that result in a higher electronic conductivity?) and indeed if the underlying mechanism that relies upon an electron-conducting support needs revisiting. The authors do imply that the alumina or zirconia layer may modify the nature of the molten carbonate (presumably by dissolution) although it is conceivable that the layers could perform this function by inhibiting silver dissolution. Permeation rates for carbon dioxide and oxygen were close to the ratio of 2:1 for the zirconia layer, but very different for the alumina layer with a ratio of 1:1.5. Further work in the case of the alumina layer membrane using Raman spectroscopy found evidence for a CO_4^{2-}-like species in the melt.[47] The occurrence of such a species was supported by favourable thermodynamics of formation from DFT calculations. The authors suggested that this species could contribute to oxygen transport through a 'cog-wheel' mechanism (Fig. 9). However, the rate of oxygen and carbon dioxide transport were much greater when both gases were present on the feed side, indicating a cooperative interaction.

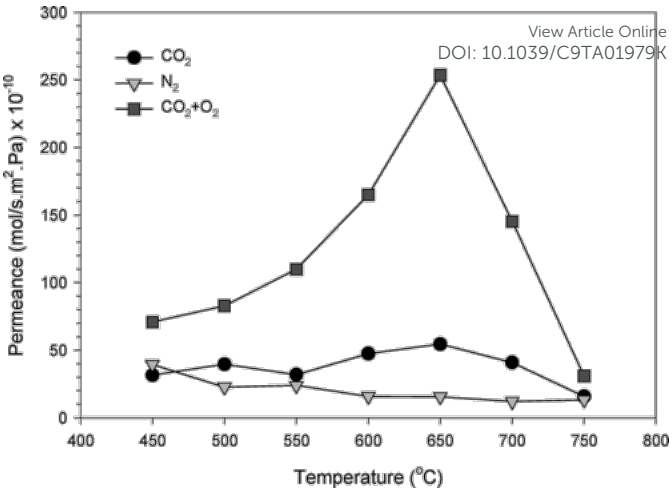

Fig. 17 – Gas permeation of carbon dioxide, nitrogen and carbon dioxide and oxygen at various temperatures from a porous stainless steel supported molten-salt membrane. Adapted from reference 76.

Chemical dealloying of Ag-Al,[99] and Ag-Zn,[100] was used to provide favourable pore structures in silver for the application of carbon dioxide capture from flue gases. In these studies, hydrogen was used in the sweep gas to reduce permeated oxygen to water. By lowering the partial pressure of oxygen, the fluxes of carbon dioxide and oxygen were improved by a factor of two. Again, the ratio of the permeation rates for carbon dioxide:oxygen was no longer equal to 2:1, but was often lower. This was also explained by the transport of the CO_4^{2-} species across the membrane and its involvement in a two-phase reaction between carbonate and oxygen. As the microstructure of the support changes, one might expect the relative rates of the three-phase and two-phase processes to change with a time-dependent effect on the carbon dioxide:oxygen ratio.

NiO was also investigated as a support for a lithium and sodium carbonate eutectic mixture.[111] The NiO pellet membrane was prepared using a carbon black pore former and subsequent infiltration. After an initial induction period of 15 hours, the resulting membrane showed good permeation rates for both carbon dioxide and oxygen in the ratio of 2:1 (Fig. 18). The presence of the induction period was explained by the formation of an interfacial reaction between the support and

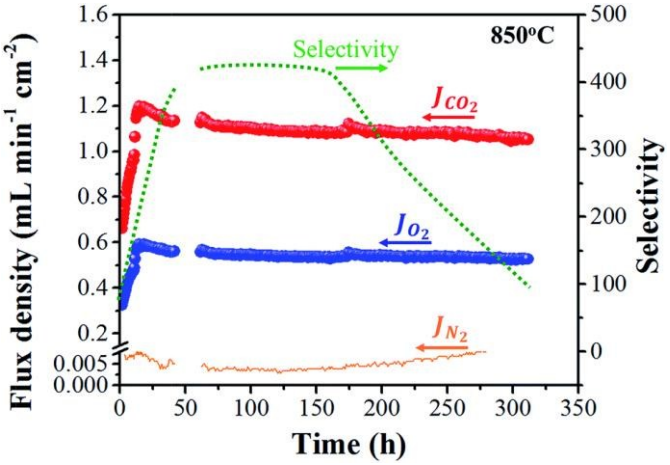

Fig. 18 – Carbon dioxide and oxygen flux densities and selectivity of a nickel oxide supported molten-salt membrane, at 850°C. Adapted from reference 111.

View Article Online
DOI: 10.1039/C9TA01970K

the molten carbonate resulting in a layer of lithiated NiO of approximately 100 nm in thickness (supported by STEM work). It was suggested that the lithiated NiO provides a route for electron transport.

Oxygen-Ion Conducting Supports

In parallel with work on nominally electron-conducting support systems there has been considerable work on oxygen ion-conducting support systems. A key publication from 2011 discussed the use of both YSZ and CGO oxygen-ion conducting supports and alumina (Fig. 19).[21] A range of alkali metal carbonate compositions were employed in the study. A 1:1 carbon dioxide:helium ratio was used in the feed gas (a 50% carbon dioxide mole fraction in inert has become a common feed gas for such studies). For some experiments carbon dioxide at 1% was also fed to the permeate side. Literature data reporting on studies where carbon dioxide is fed to the permeate side remains rare.[iv] A pure lithium carbonate and YSZ membrane was shown to fail, probably due to zirconate formation. Hence, a YSZ membrane with sodium and potassium carbonate (reduced reactivities are expected relative to lithium carbonate) was utilised. These membranes reached carbon dioxide permeabilities of 10^{-11} mol m^{-1} s^{-1} Pa^{-1} (or permeance of 3 x 10^{-8} mol m^{-2} s^{-1} Pa^{-1}) at 850°C. There was no evidence of interfacial reactions in the case of a CGO support, yet permeabilities were somewhat lower than for YSZ. YSZ-supported membranes have also been employed in hollow fibre form,[105] with similar permeabilities to those previously reported for YSZ pellet membranes.[21] There have been a number of additional papers that have used oxygen-ion conducting ceria supports such as CGO and SDC.[55,57,97,107,112–117] Of particular note are papers concerning the formation of interconnected 3D pore networks that yielded permeabilities in excess of 10^{-11} mol m^{-1} s^{-1} Pa^{-1} even at temperatures as low as 600°C, and the use of a supported wetting SDC layer (150 microns in thickness) on a non-wetting support, that reduced the effective diffusional path length and achieved greater fluxes. Finally, adding steam to the sweep gas of a ceria-supported molten carbonate membrane resulted in a two orders of magnitude increase in carbon dioxide flux with carbon dioxide permeabilities of 10^{-12} mol m^{-1} s^{-1} Pa^{-1}. The promotional effect was attributed to the additive contribution of hydroxide ions in the melt and oxygen ions in the support to a counter-current transport mechanism (Fig. 5b).[55]

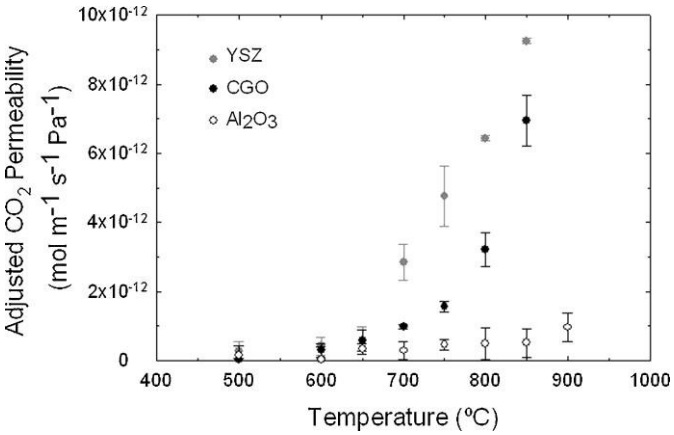

Fig. 19 – Carbon dioxide permeability for YSZ, CGO and alumina supported molten-salt membranes. Membrane thickness ranged from 200 to 400 µm. Adapted from reference 21.

Mixed Ion-Electron Conducting Supports

As well as studying both electron-conducting and oxygen-ion conducting supports a number of studies have involved the use of mixed ionic and electronic conducting supports (MIECs). The majority of these papers have involved the use of LSCF.[62,63,86,106] Many of the papers that employ MIEC supports interpret their behaviour in terms of oxygen-ion conductivity in the support and carbonate conductivity in the molten salt. However, these papers tend to look only at the permeation of carbon dioxide in the absence of any other potentially reactive gases and not, *e.g.* the permeation of carbon dioxide in the presence of oxygen or indeed of oxygen alone. Thus, the experimental data set is somewhat more limited than would be desired. Other results have been interpreted in light of both oxygen-ion and electron conduction being important in the support.[118] Metcalfe *et al*. were able to use an LSCF-supported membrane to permeate carbon dioxide 'uphill' against its chemical potential difference using an oxygen chemical potential driving force.[110] Clearly, this would not be possible if the oxygen-ion conductivity of the support were relatively high. So, we probably have a rather complex picture in the case of MIEC supports where the conditions of the experiments (relative partial pressures of *e.g.* carbon dioxide and oxygen) and nature of the experiments (*e.g.* oxygen present or not) influence the membrane behaviour and its state and evolution.

3.2 Molten Salt & Support Materials Compatibility

Typical supported molten-salt membrane permeation experiments very rarely go beyond ~300 hours and they do not investigate in detail the stabilisation periods routinely observed over a number of hours at the beginning of experiments. These transient permeation periods are likely due, at least in part, to the formation of new interfaces. Also, for long-term operation it will be necessary to investigate supported molten-salt membranes under conditions as close to application as possible. Currently, the majority of permeation experiments use unrealistic feed-gas compositions useful for comparison, but far from the reality of the intended application. Furthermore, more detailed investigations related to materials compatibility will be required, particularly at the solid-liquid and solid-gas interfaces. Here, we review the limited literature focussed on such issues of importance to long-term operation.

[iv] However, such an approach can be extremely valuable if one wishes to use permeation rates to draw conclusions about mechanism, as in the presence of relatively small permeation rates, permeate side gas composition can be known and controlled. Conventional experiments may result in an uncharacterised and indeed variable permeate side pCO_2 that will be correlated to permeation rate with obvious potential problems. However, the determination of permeation rate is now more difficult as a result of the background carbon dioxide mole fraction on the permeate side.

View Article Online
DOI: 10.1039/C9TA01070K

Solid-Liquid Interface

Molten carbonate and certain metals or metal oxides are chemically unstable when in contact with each other at high temperature.[119] The dissolution of solids in molten carbonates is influenced by the acid-base character of the melt (in these melts, the oxide ion defines basicity, in the same way that the hydrogen ion defines acidity in aqueous solutions). Take NiO as an example of a simple metal oxide, relevant due to its use as a support for molten-salt membranes.[111] Dissolution products are dependent on the oxygen-ion activity, which is in turn dependent on the pCO_2 of the molten-salt environment. When pCO_2 is high, dissolution products are Ni^{2+} complexes, with NiO_2^{2-} complexes presenting when pCO_2 is low. To complicate matters further, NiO^- or NiO_3^{2-} may be present in the latter case as well. As the feed and permeate-sides of these membranes will be exposed to high and low pCO_2 respectively, a chemical potential gradient of such species within the melt may form, and in turn their permeation could be anticipated. To the authors' best knowledge, studies on the impact of species from support dissolution on membrane performance has not started. Therefore, we restrict the following discussion to solid products observed at the liquid-solid interface.

In one of the first reported supported molten-salt membranes, supported with stainless steel, the formation of $LiFe_5O_8$ and $LiFeO_2$ resulted in a decrease in electronic conductivity and, concurrent reduction in carbon dioxide permeation.[76] Similarly, in YSZ, zirconia reacts to form lithium zirconate, decreasing electronic conductivity and inhibiting carbon dioxide flux.[21,120] In LSCF membranes, it has been postulated that lithium cobalt oxide forms at the interface,[86] and with alumina it is long-established that lithium aluminate forms (indeed, lithium aluminate has been used to construct molten carbonate fuel cells due to its limited reactivity with molten carbonate). Silver does not form interfacial phases although,[79] as above, alumina and zirconia layers have been deposited on the surface to improve wettability.[64,82] These layers will then transform to their lithiated counterparts. CGO appears to show excellent stability in contact with molten carbonate,[21] although the techniques used to reach this conclusion (XRD and TGA) do not possess the surface sensitivity required to reach such a conclusion about interfacial species, potentially present as ~nm scale layers at the surface.

Solid-Gas Interface

At the solid-gas interface, a lot more is known about the stability of the supports as many have been applied as catalyst supports and/or membranes for *e.g.* oxygen separation. For example, the kinetic de-mixing effect in perovskites for oxygen separation is well known. Here, we limit ourselves to the impact of the interaction between gas phase species likely present in carbon dioxide separations and supports for molten-salt membranes.

The alkaline metals of MIEC supports are thermochemically unstable under a carbon dioxide atmosphere at elevated temperatures. In LSCF, reaction with carbon dioxide results in the formation of strontium carbonate at the surface. The loss of the A-site La, leads to secondary formation of cobalt oxide at the surface. With oxygen present, strontium carbonate becomes unstable, and the perovskite structure is retained (Fig. 20).[62] The formation of a carbonate layer at the membrane surface may well impact performance as, if present at the triple-phase-boundary, it could retard the transport of oxygen-ions or electrons between the phases (Fig. 5). Removing the alkaline metals can lead to greater stability, but at the cost of lower permeation rates. LCGFA supported molten-salt membranes show lower carbon dioxide permeation, yet are thermo-chemically stable under a range of gas atmospheres.[88] In SDC supported molten-salt membranes, long-term stability in carbon dioxide has been observed, yet with hydrogen present, support decomposition was apparent.[112]

Typically, supported molten-salt membranes for carbon dioxide permeation are exposed to a feed gas containing carbon dioxide in nitrogen, with an inert sweep gas. Although useful for

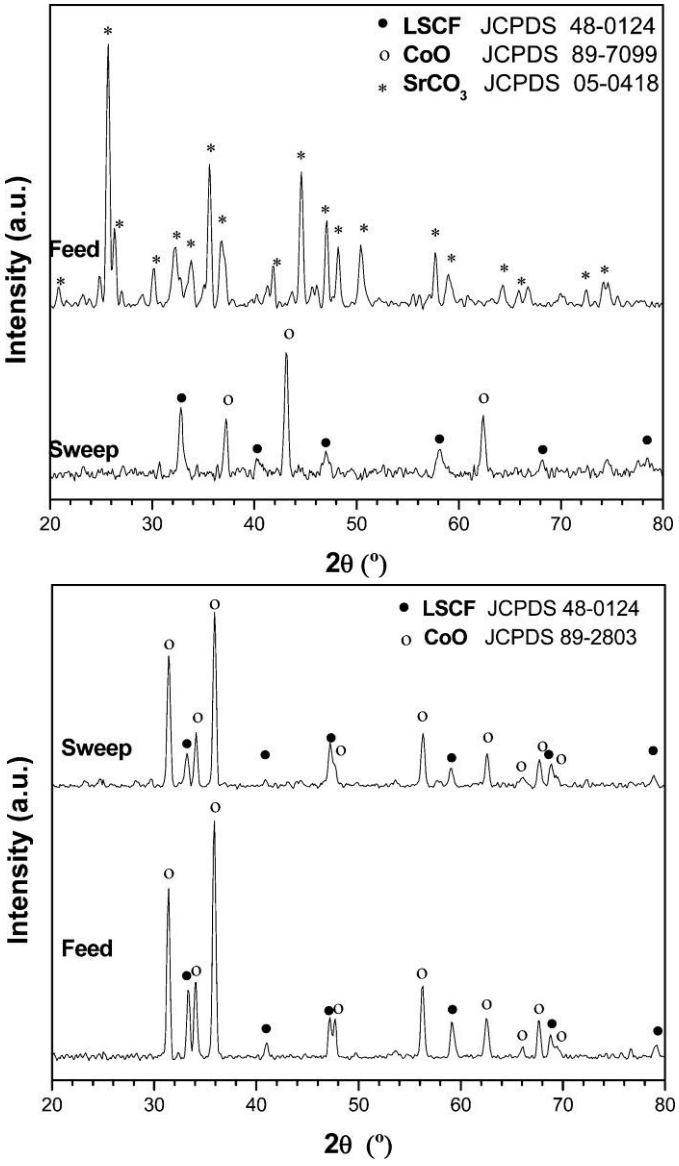

Fig. 20 – XRD diffractograms of LSCF supported molten-salt membranes exposed to carbon dioxide and nitrogen (top) and carbon dioxide and oxygen (bottom) at temperatures ranging from 850 to 950 °C for 110 and 600 hours respectively. Phases identified by JCPDC file numbers. Adapted from reference 62.

View Article Online
DOI: 10.1039/C9TA01979K

comparing experiments between laboratories, the composition does not reflect the majority of intended applications. For example, a typical pre-combustion gas may contain hydrogen sulfide impurities. In a post-combustion flue gas, there may be sulfur dioxide.[121] Steel- and silver-supported membranes may react with hydrogen sulfide to form metal sulfides. The reaction reduces the active thickness of the support, and in steel, the atomic hydrogen by-product diffuses into the bulk and combines to form molecular hydrogen. The associated pressure build-up eventually leads to fracture and failure, a phenomenon known as sulfide stress cracking.[122,123] In silver, even at <5 ppm hydrogen sulfide, in the presence of moisture, silver sulfates form at the surface, reducing the electronic conductivity.[124]

Ceramic supported molten-salt membranes are also affected by the presence of gaseous sulfur compounds. Sulfur dioxide chemisorbs on alumina surfaces to form adsorbed sulfite, subsequently oxidised to aluminium sulfate.[125] Adsorption is not completely reversible, with cumulative loss of adsorption capacity after regeneration cycles. A theoretical model based on a combination of DFT and thermodynamic data suggested that cerium sulfate readily forms on the surface of ceria exposed to sulfur dioxide.[126] Chen *et al.*, observed hydrogen sulfide poisoning of SDC supported molten-salt membranes.[127] Hydrogen sulfide had a negligible effect on the carbonate phase (~0.4 wt% sulfur in the carbonate region determined by EDX), yet carbon dioxide flux decreased with increasing hydrogen sulfide concentration (50 – 200 ppm). Hydrogen sulfide did not permeate the supported molten-salt membrane during ~30 hours of membrane operation, indicating selectivity was maintained, but the carbon dioxide flux decrease was severe and increased with increasing hydrogen sulfide concentration. Similar effects on carbon dioxide flux were observed for the same membrane exposed to sulfur dioxide however, the detrimental effect was related to conversion of the molten carbonate to sulfate, this time with limited effect on the support (~0.2 wt% S in the SDC region determined by EDX).[128] LSCF membranes for oxygen separation show an irreversible decrease in oxygen flux of up to 80% with the addition of sulfur dioxide, depending on operation temperature.[129] With hydrogen sulfide exposure, similar oxygen flux reductions were observed.[130] In both cases, the authors suggested the formation of strontium sulfate at the surface was likely responsible for the oxygen flux decrease.

It is important to point out that few of the studies mentioned above are observing effects in supported molten-salt membranes; currently, information must be taken from disparate fields and combined in an attempt at a full picture. Furthermore, a large range of potential application-specific conditions would imply that testing should be performed under gas atmospheres representative of the target application.

As a final comment on long-term stability, we have not discussed sealing issues. In general, ceramic membrane sealing is a complex feature of the membrane module, complicated further in this case by the presence of corrosive and creeping molten salts. Creeping carbonates can be replenished, as has been achieved previously for molten carbonate fuel cells, but this adds further operating costs. Ideally, creep would be mitigated by appropriate membrane design, and the use of manifold and sealant materials that are non-wetting and unreactive with molten carbonate. Finally, expansion or contraction upon the formation of secondary phases may well mechanically stress both the membrane and the seals further.

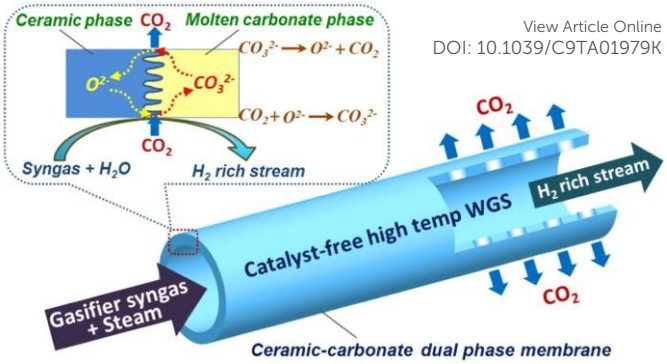

Fig. 21 – Schematic of a supported molten-salt membrane reactor for carbon dioxide removal from the water-gas-shift reaction. Adapted from reference 132.

3.3 Alternative Supported Molten-Salt Concepts and Applications

Due to the ability of supported molten-salt membranes to operate at high temperature, they are beginning to be tested for application in separation-enhanced reactions. Also, we have thus far focussed on molten carbonate supported molten-salt membranes. Alternative molten salts may be used, applied as membranes or adsorbents. Here we discuss separation enhancement using supported molten-salt membranes, alternative gas separations and supported molten-salt adsorbents.

Supported Molten-Salt Membrane Reaction Engineering

Separation-enhanced reaction processes involve the selective removal of a reaction product, to drive equilibrium towards a desired product.[131] For hydrogen production, the concept involves removal of carbon dioxide from the water-gas-shift reaction ($CO + H_2O = H_2 + CO_2$). The reaction is equilibrium limited, meaning it is impossible to fully convert carbon monoxide without separation enhancement. The first demonstration of this concept using a supported molten-salt membrane was by Lin *et al.*, where they achieved a carbon monoxide conversion of ~26% by performing ~19% carbon dioxide recovery (carbon dioxide flux of 2.7 x 10^{-3} mol m^{-2} s^{-1}) in a symmetric tubular SDC membrane at 900°C (Fig. 21).[132] The choice of SDC was likely stimulated by the excellent stability under simulated syngas (50% CO, 35% CO_2, 10% H_2, and 5% N_2); 35 days with minimal performance decrease at 700°C.[112] Further testing of the concept, separating carbon dioxide from a simulated syngas using asymmetric tubular membranes, provided a higher carbon dioxide flux (1.21 x 10^{-2} mol m^{-2} s^{-1} at 900°C).[108]

Dry methane reforming ($CH_4 + CO_2 = 2CO + 2H_2$) has also been performed using supported molten-salt membranes. The process removes carbon dioxide from a mixed gas feed-stream, before release from the permeate side into a stream of methane. A methane reforming catalyst is deposited on the permeate-side of the membrane (Fig. 22). Combining carbon dioxide separation from *e.g.* flue gases and dry methane

View Article Online
DOI: 10.1039/C9TA01979K

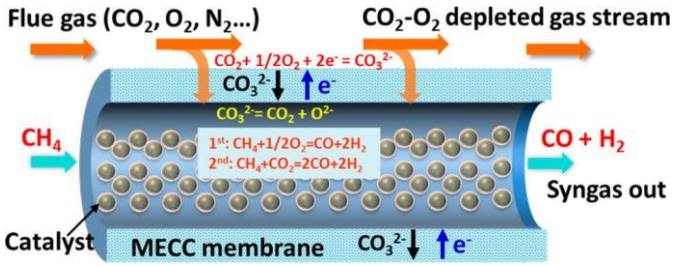

Fig. 22 – A combined carbon dioxide capture and catalytic methane reforming membrane process. Carbon dioxide and oxygen are separated from a flue gas mixture and injected into a permeate-side stream of methane. Adapted from reference 135.

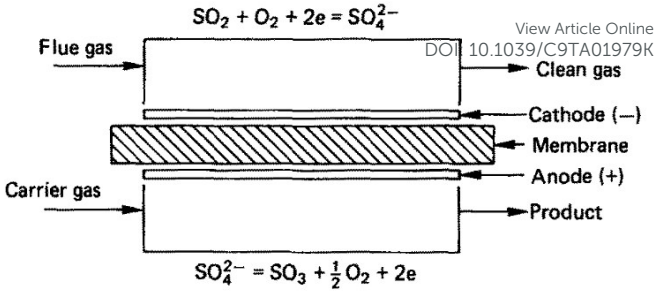

Fig. 23 – Schematic of an electrochemical membrane for sulfur dioxide separation from flue gas, with cathodic and anodic reactions shown. Adapted from reference 140.

reforming in one reactor provides process intensification and potentially cost reduction. Furthermore, heat from the flue gas can be used to provide energy input for the endothermic reforming reaction. The first demonstration of the concept used an LSCF pellet with a nickel/alumina catalyst deposited on the permeate-side. Although the concept was demonstrated, the methane conversion and syngas production rate was low at ~8% and <1.0 mL min^{-1} cm^{-2} respectively.[133] More recent studies have improved the concept, by changing membrane material and structure, as well as catalyst. A GDC membrane with a Ni-MgO-1wt% Pt catalyst achieved methane conversion of 94% and syngas production rates of >3 mL min^{-1} cm^{-2}.[134] A zirconia-coated silver membrane achieved syngas production rates of >4 mL min^{-1} cm^{-2}.[135] In the latter case, using an electronically-conductive membrane, the co-permeation of oxygen was also found to reduce coking of the catalyst on the permeate-side (Fig. 22).

Although still at proof-of-concept stage, interest in performing reactions with supported molten-salt membranes is likely to continue to attract attention, due to a lack of effective materials for high-temperature carbon dioxide separation.

Alternative Permeations

The supported molten-salt membrane concept is clearly not limited to molten carbonate, although the recent literature is dominated with these examples. A small body of work by Winnick *et al*. details the electrolytic membrane concept, whereby a supported molten-salt (*e.g.* molten sulfate) is held between two porous electrodes (Fig. 23). The concept was demonstrated for hydrogen sulfide removal from fuel gases,[136–138] sulfur oxides separation and,[139–141] the separation of halogens from hydrogen halide gas streams[142–145] demonstrating the wide potential utility of supported molten-salt membranes by changing the molten salt.

More recently, Metcalfe *et al*. reported nitrogen oxide membranes, using a potassium nitrate salt in both alumina and LSCF. The former showed no oxygen permeation when fed with a mixture of carbon dioxide, nitrogen dioxide and oxygen. No carbon dioxide permeation was observed, with only nitrogen dioxide permeating in the alumina membrane, and both nitrogen dioxide and oxygen permeation in the LSCF membrane. Overall, a permeance of 6.9 x 10^{-8} mol m^{-2} s^{-1} Pa^{-1} was achieved.

Returning to carbon dioxide permeation, a recent study showed that replacing molten carbonate with molten hydroxide resulted in carbon dioxide permeabilities one order of magnitude higher than the best supported molten-carbonate membranes, i.e. 10^{-10} mol m^{-1} s^{-1} Pa^{-1} at 650 °C.[56] Furthermore, at <400 °C, permeability remained high at 10^{-11} mol m^{-1} s^{-1} Pa^{-1}, rivalling molten carbonate membranes whilst lowering the operating temperature. The molten hydroxide mixture employed melts at ~190 °C and maintains a high ionic conductivity across a wide temperature range (1 – 3 S cm^{-1} at 250 – 650 °C); by translating the counter-current transport of oxygen ions normally occurring in the solid support (Fig. 5b) to hydroxide ions within the molten salt, a simultaneous reduction in operating temperature and improvement in flux was realised. The molten hydroxide composition initially employed will change with time, converting to molten carbonate in the presence of carbon dioxide. In this work, molten carbonate accounted for 10-90 mol % of the molten salt, depending on the conditions employed.[56]

Supported Molten-Salt Adsorbents

The combination of a porous inorganic solid and a molten salt for carbon dioxide separation is not limited to membrane fabrication. The application of metal oxides (*e.g.* magnesium or calcium oxide) as carbon dioxide capture adsorbents is well-documented, with pilot plants in operation (Fig. 2). Supported molten-salt adsorbents have been shown to tackle some outstanding issues of metal oxide adsorbents: low capacities (magnesium oxide), slow adsorption/desorption kinetics and, the formation of carbonate product layers that retard further carbonate formation.

A typical supported molten-salt adsorbent is magnesium oxide with a molten alkali nitrate salt dispersed on the surface. In the case of an adsorbent it is desirable for the solid and molten phases to react with carbon dioxide. The salt enhances both the capacity of the sorbent overall, and the kinetics, acting as a phase-transfer catalyst (Fig. 24).[146] Magnesium oxide dissolves into the molten salt to form solvated ionic pairs ($Mg^{2+}\cdots O^{2-}$). Adsorbed carbon dioxide reacts at the gas-liquid-solid triple-phase-boundary to form a ($Mg^{2+}\cdots CO_3^{2-}$) pair. As the carbonate can precipitate elsewhere, the formation of a carbonate layer does not retard further carbonation, enhancing overall capacity.[146,147] Consequently, molten salts can typically increase magnesium oxide capacity from <1 mmol g^{-1} to >10 mmol g^{-1}. The alternate reaction pathway (Fig. 24), also improves reaction kinetics. In an elegant model experiment, the high concentration and conductivity of oxygen ions in nitrate salts was shown to rapidly form calcium carbonate on a calcium oxide adsorbent and provide easier regeneration.[148] Desorption

View Article Online
DOI: 10.1039/C9TA01979K

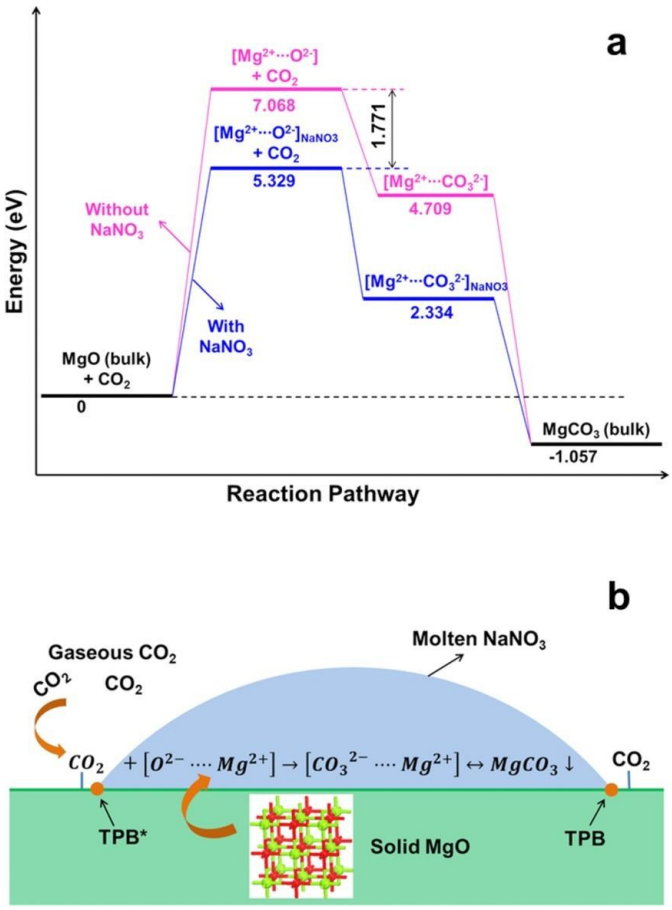

Fig. 24 – Reaction pathway and mechanism for a supported molten-salt adsorbent. Adapted from reference 146.

(or dissociation of carbonate ions) is accelerated due to favourable solvation of the produced oxygen ion in the molten salt. A more comprehensive review on supported molten-salt adsorbents has been published.[149]

4. Commercialisation and Scale-Up of Supported Molten-Salt Membranes

There is limited open information on scaling-up and commercialisation of supported molten-salt membranes, which point however, to promising evidence of their potential in various separation processes, as indicated below. We also highlight challenges which require active research and development to foster the industrial deployment of these membranes.

4.1 Process Integration

Although supported molten-salt membrane processes are still in their infancy, a few studies have investigated possible scenarios for integration of these membranes in carbon dioxide separation in power generation. For example, several process integration studies of supported molten-carbonate membranes were performed for an Integrated Gasification Combined Cycle (IGCC) and a Natural Gas Combined Cycle (NGCC) in a 400 MW power plant.[150] These cases represented a wide range of capture conditions, *i.e.* flue gas from NGCC post-combustion process with very low carbon dioxide partial pressure and low temperature (400 - 450°C), and IGCC pre-combustion process with high carbon dioxide partial pressure and higher temperature (550 - 650°C). Within the boundary conditions set in this study, the results showed that the supported molten-salt membrane concept for carbon dioxide/nitrogen separation has a higher energy penalty (2.5 – 3.5%) than an amine-based post-combustion capture process. This was explained by the compression work required to compress the feed stream and steam extraction for sweep flow to ensure sufficient driving force across the membrane. However, the study showed that the membranes out-performed the reference Selexol technology for pre-combustion carbon dioxide capture from an IGCC process. The Shell-type gasifier with Selexol unit for carbon dioxide (and hydrogen sulfide) capture used as the reference case and a cryogenic air separation unit produced oxygen to the gasifier and inert nitrogen for use as diluent in the power island (gas turbine, heat recovery *etc.*). Six process concepts were evaluated, in which the membrane process to remove carbon dioxide was placed in front of the Selexol unit (now used only for hydrogen sulfide removal after the membrane). It was found that the overall process efficiency of the supported molten-salt membranes was higher with about 0.8 – 2.15% improvement. These results highlight the potential of these membranes in carbon dioxide capture technologies, as also demonstrated in other studies.[151,152] We note however, that issues surrounding the effect of flue gas impurities on membrane performance have not been studied in detail. A small number of studies, on *e.g.* the effect of sulfur dioxide and hydrogen sulfide, can be found in the literature.[127,128] However, current approaches for fly ash and mercury removal require flue gas cooling. This implies that supported molten-salt membranes would either have to remain functional in the presence of these contaminants at high temperature, or cooling of flue gases, before subsequent re-heating and introduction to supported molten-salt membranes would be required.

4.2 Manufacturability and Scale-Up

As reported above, the majority of the work on supported molten-salt membranes has focussed on disk-shaped membranes (pellets of a few cm^2 area). Two main processing routes are often reported. A porous ceramic support is pre-formed using pore forming agents and sintering to create the porous network (Section 2.3). The molten salt is then infiltrated by soaking the porous ceramic in the hot melt. It is critical to ensure that the ceramic is pre-heated before the infiltration takes place to avoid crystallisation of the molten salt at the supports surface.[38,108] The excess of molten salt is then removed prior to operation of the membrane by *e.g.* polishing. The degree of infiltration will depend on the wettability and pore size of the support, as well as the pressure difference applied over the membrane (Equation 4) (Fig. 8). To facilitate infiltration of the molten salt in microstructured ceramics, vacuum can also be used during the soaking step. As an alternative to this process, the powders of the support and salt materials are mixed together and cold-pressed, followed by annealing to form the composite membranes. While the former process

View Article Online
DOI: 10.1039/C9TA01979K

gives in general mechanically strong membranes, the latter yields composites with lower mechanical strength due to the lower annealing temperature applied to consolidate the membranes.

Membranes with a larger active surface area have also been produced using porous tubular supports, hollow fibre supports as well as asymmetric planar and tubular architectures, where the thinner supported membrane is deposited on a porous mechanical support.[38,105,108] Examples of techniques used for manufacturing the supports include extrusion, tape-casting, isostatic pressing, centrifugal casting, the phase inversion method, spinning and slip-casting, which can be used for the production of larger volumes of membrane supports. In the majority of cases, the pre-formed ceramic is soaked in molten salt, with the excess again polished or wiped off. Currently, the production of supported molten-salt membranes is confined to laboratory scale, and there is no information on production yield or reproducibility. However, the scale-up of these membranes could realistically be envisaged, considering the significant knowledge base and existing infrastructure for manufacturing of related systems such as molten carbonate fuel cells (MCFCs) and porous functional ceramics. Both of these have reached a much higher level maturity with *e.g.* MCFCs reaching pilot scale with development projects of several hundred kW since early 2000, and MW systems today.

Further work on these systems should be directed towards the development of low-cost manufacturing routes with robust process control parameters and high roll-out yield. In this respect, one may consider that controlling the infiltration of the molten phase in asymmetric architectures is not trivial to implement at large scale, while achieving the desired microstructural characteristics of the produced membranes (*e.g.* regarding the targeted thickness). As reported earlier, a suitable selection of wetting and non-wetting materials for the porous ceramics could mitigate this issue and help with confining the molten phase infiltration to the desired porous ceramic layer.[94,107,108] This strategy would also contribute to reduce long-term molten salt creep.

Further challenges hamper the deployment of supported molten-salt membranes at commercial scale. Despite significant improvement of performance reported over the past decades, there is limited data on long term performance in process-relevant conditions. This is in part due to the need for more fundamental research aiming at further understanding of transport mechanisms in these systems, in line with the search for compatible materials for the solid and liquid phases. Furthermore, limited activity has been devoted to the design and development of reactor concepts for handling the corrosive environment produced by molten salts and integrating sealing technology to enable *e.g.* high-pressure measurements. There is, however, a necessity to carry out such experimental investigation to provide feedback for further optimisation of materials and membrane design, as well as to establish lifetime prediction models. For example, long-term creep is a critical challenge for molten salt based systems and is affected by the physico-chemical properties of the membranes, hardware materials in contact with the membranes (*e.g.* reactor piping and seals) and the operational parameters.

4.3 Stability and Long-Term Testing

As commented above (Section 3.2), supported molten-salt membrane permeation experiments in the open literature rarely go beyond ~300 hours of operation. To predict the lifetime of these membranes, far longer experiments should be pursued. We conclude this section with unpublished results representing the longest supported molten-salt membrane permeation experiment reported to date, of ~2000 hours (unpublished results courtesy of SINTEF). The stability of a ceria-supported molten-carbonate pellet membrane (with the addition of 5 wt% copper oxide in the molten carbonate) was investigated under various operating conditions (Fig. 25). The membrane was first tested for ~1 month in inert or oxidising atmospheres (containing carbon dioxide, helium, nitrogen or oxygen, not included in Fig. 25), and subsequently in the presence of 20% hydrogen, which is relevant for application of the membrane in pre-combustion carbon dioxide capture processes.

When hydrogen was supplied in the feed gas mixture, the carbon dioxide flux first increased due to formation and dissolution of steam and, hydroxide ion transport. This effect was observed and discussed in detail previously.[55] After the initial carbon dioxide flux increase, the flux was relatively stable for ~500 hours after which a gradual decrease was evidenced for the following ~1000 hours. The rate of flux degradation accelerated at ~1500 hours. The subsequent increase in operating temperature to 575 and 600°C initially led to an increased carbon dioxide flux, followed by a more drastic flux decrease. At ~1750 hours, 2.5% steam was introduced to the membrane permeate side. Whereas the carbon dioxide flux increased when steam was introduced to the sweep side, it quickly returned to its prior value after removal of the steam. The carbon dioxide flux continuously decreased until the lower detection limit for the analytical apparatus was reached at

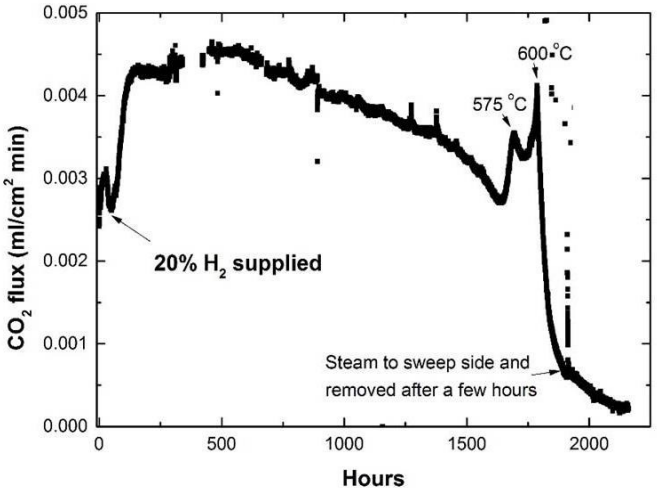

Fig. 25 – Long-term stability testing for a ceria-supported molten carbonate membrane with 5 wt% copper oxide dissolved in the molten carbonate under inert and reducing atmospheres. The membrane had been operated for ~1 month before hydrogen was introduced.

View Article Online
DOI: 10.1039/C9TA01979K

~2200 hours. It should be mentioned that the membrane remained gas-tight during this experiment, as evidenced by the use of helium in the feed gas mixture as a leak detection agent.

Conclusions

Supported molten-salt membranes show promise for carbon dioxide permeation, in a range of economically and environmentally significant separations and, at temperatures where other membrane materials and ab/adsorption processes face significant limitations. These advantages are largely due to intrinsic properties of the membrane materials (*e.g.* theoretically infinite selectivity *via* facilitated-transport and high diffusivities in the molten phase leading to high fluxes). We may conclude by elaborating on some of the issues that seem to lead to complexity for this class of membrane.

Firstly, there is a lack of reliable information on fundamental properties of the molten salt, *e.g.* gas solubility and molten salt speciation (Section 2.1). Such information, both experimental and computational, would prove invaluable in designing new separation processes and determining permeation mechanisms (Section 3). Investigations of molten carbonate wettability on various support materials, and under a variety of conditions, would help in the design of membrane modules, particularly to limit long-term molten salt creep (Section 2.1 and 4.3). Although a number of synthetic methods to tailor support microstructure have been applied (Section 2.3 and 4.2), it seems particularly obvious that reducing the support thickness as far as possible, whilst maintaining practicable mechanical strength, would result in carbon dioxide permeances competing with, and bettering, the most promising carbon dioxide permeable membranes. Regarding support materials, a change in direction may be required (Section 2.2 and 3.2). Instead of aiming for supports with increasingly higher conductivities, a focus on maintaining good performance over longer periods of time, may be more useful. It would also likely appear that an interfacial solid phase may form, that the composition of this may change and that this region may grow during operation (Section 3.1 and 3.2). The nature of this region may be influenced not only by the melt composition but also the gas phase composition. The melt composition itself may also change and may in particular be influenced by the gas phases; speciation in the melt is likely to be complex with many more active species present than simply carbonate, particularly when gases other than carbon dioxide are considered *e.g.* steam or SO_2 (Section 2.1, 3.2 and 4.3). Furthermore, membrane structure will evolve (Section 3.2), highlighting the need for far longer permeation experiments (Section 4.3). The simple models presented in Fig. 5 and discussed in Section 3.1 are undoubtedly an oversimplification and unlikely to explain performance, particularly as experimental datasets increase in size and begin to include a wider range of experiments for different applications (Section 3.3 and 4.1). Finally, the experiments employed are often too narrow in scope to probe the detailed chemistry likely to be occurring.

We would suggest that the level of complexity encountered is to be expected given the properties of the phases involved. To realise the potential of supported molten-salt membranes, this complexity should be embraced.

Conflicts of interest

There are no conflicts to declare.

Acknowledgements

The research leading to these results has received funding from the European Research Council under the European Union's Seventh Framework Programme (FP/2007-2013) / ERC Grant Agreement Number 320725 and from the Engineering & Physical Sciences Research Council (EPSRC) *via* grants EP/M01486X/1, EP/P007767/1 and EP/P009050/1, as well as from the MOCO3 project (272688) granted by the Research Council of Norway through the M-ERA.NET program. G.A.M. would like to thank the EPSRC for a Doctoral Prize Fellowship (EP/M50791X/1).

Notes and references

1 T. Gasser, C. Guivarch, K. Tachiiri, C. D. Jones and P. Ciais, *Nat. Commun.*, 2015, **6**, 1–7.
2 D. S. Sholl and R. P. Lively, *Nature*, 2016, **532**, 435–437.
3 M. Bui, C. S. Adjiman, A. Bardow, E. J. Anthony, A. Boston, S. Brown, P. S. Fennell, S. Fuss, A. Galindo, L. A. Hackett, H. J. Herzog, G. Jackson, J. Kemper, S. Krevor, G. C. Maitland, M. Matuszewski, I. S. Metcalfe, C. Petit, G. Puxty, J. Reimer, D. M. Reiner, E. S. Rubin, S. A. Scott, N. Shah, B. Smit, J. P. M. Trusler, P. Webley, J. Wilcox and N. MacDowell, *Energy Environ. Sci.*, 2018, **11**, 1062–1178.
4 T. C. Merkel, H. Lin, X. Wei and R. Baker, *J. Memb. Sci.*, 2010, **359**, 126–139.
5 G. T. Rochelle, *Science (80-.).*, 2009, **325**, 1652–1654.
6 R. S. Haszeldine, *Science (80-.).*, 2009, **325**, 1647–1652.
7 S. Choi, J. H. Drese and C. W. Jones, *ChemSusChem*, 2009, **2**, 796–854.
8 B. Arias, M. E. Diego, J. C. Abanades, M. Lorenzo, L. Diaz, D. Martinez, J. Alvarez and A. Sanchez-Biezma, *Int. J. Greenh. Gas Control*, 2013, **18**, 237–245.
9 M. Chang, W. Chen, C. Huang, W. Liu, W. Chang, W. Chen, J. Cheng, K. Huang and H. Hsu, *Energy Procedia*, 2014, **63**, 2100–2108.
10 H. A. J. Van Dijk, P. D. Cobden, M. Lundqvist, C. C. Cormos, M. J. Watson, G. Manzolini, S. Van Der Veer, L. Mancuso, J. Johns and B. Sundelin, *Energy Procedia*, 2017, **114**, 6256–6265.
11 S. Tonomura, *Energy Procedia*, 2013, **37**, 7160–7167.
12 C. Gebald, J. A. Wurzbacher, P. Tingaut, T. Zimmermann and A. Steinfeld, *Environ. Sci. Technol.*, 2011, **45**, 9101–9108.
13 T. Nguyen, *Chem. Eng. News*, 2017, 15.
14 D. W. Keith, G. Holmes, D. St. Angelo and K. Heidel, *Joule*, 2018, **2**, 1–22.
15 D. M. D'Alessandro, B. Smit and J. R. Long, *Angew. Chemie* -

Int. Ed., 2010, **49**, 6058.
16 L. M. Robeson, *J. Memb. Sci.*, 2008, **320**, 390–400.
17 N. Bryan, E. Lasseuguette, M. Van Dalen, N. Permogorov, A. Amieiro, S. Brandani and M. C. Ferrari, *Energy Procedia*, 2014, **63**, 160–166.
18 C. A. Trickett, A. Helal, B. A. Al-Maythalony, Z. H. Yamani, K. E. Cordova and O. M. Yaghi, *Nat. Rev. Mater.*, 2017, **2**, 1–16.
19 L. M. Robeson, M. E. Dose, B. D. Freeman and D. R. Paul, *J. Memb. Sci.*, 2017, **525**, 18–24.
20 S. Frangini and A. Masi, *Int. J. Hydrogen Energy*, 2016, **41**, 18739–18746.
21 J. L. Wade, C. Lee, A. C. West and K. S. Lackner, *J. Memb. Sci.*, 2011, **369**, 20–29.
22 J. Dupont, *Acc. Chem. Res.*, 2011, **44**, 1223–1231.
23 C. Maton, N. De Vos and C. V Stevens, *Chem. Soc. Rev.*, 2013, **42**, 5963–5977.
24 G. J. Janz and M. A. X. R. Lorenz, *J. Chem. Eng. Data*, 1961, **6**, 321–323.
25 R. I. Olivares, C. Chen and S. Wright, *J. Sol. Eng.*, 2017, **134**, 1–8.
26 X. An, J. Cheng, P. Zhang, Z. Tang and J. Wang, *Faraday Discuss.*, 2016, **190**, 327–338.
27 P. Claes, D. Moyaux and D. Peeters, *Eur. J. Inorg. Chem.*, 1999, **3**, 583–588.
28 P. L. Spedding and R. Mills, *J. Electrochem. Soc.*, 1965, **112**, 594–599.
29 M. S. Bohn and G. J. Janz, *J. Chem. Eng. Data*, 1987, **32**, 180–182.
30 S. W. Kim, K. Uematsu, K. Toda and M. Sato, *J. Ceram. Soc. Japan*, 2015, **3**, 355–358.
31 J. Kestin, M. Sokolov and W. A. Wakeham, *J. Phys. Chem. Ref. Data*, 1978, **7**, 941–948.
32 R. Alcalde, G. Garc, M. Atilhan and S. Aparicio, *Ind. Eng. Chem. Res.*, 2015, **54**, 10918–10924.
33 T. Kojima, Y. Miyazaki, K. Nomura and K. Tanimoto, *J. Electrochem. Soc.*, 2008, **155**, 150–156.
34 M. Tanaka, G. Girard, R. Davis, A. Peuto and N. Bignell, *Metrologia*, 2001, **38**, 301–309.
35 K. Igarashi, K. Tajiri, T. Asahina and M. Kosaka, *Zeitschrift fur Naturforsch. A*, 1992, **47**, 675–677.
36 P. Nikolopoulos, *J. Mater. Sci.*, 1985, **20**, 3993–4000.
37 A. Tsoga and P. Nikolopoulos, *J. Mater. Sci.*, 1996, **31**, 5409–5413.
38 B. Lu and Y. S. Lin, *J. Memb. Sci.*, 2013, **444**, 402–411.
39 T. Yokokawa, *Pure Appl. Chem.*, 1986, **58**, 1547–1552.
40 R. P. T. Tomkins and N. P. Bansal, *Gases in Molten Salts (IUPAC Solubility Data Series)*, 1991.
41 A. J. Appleby and C. Van Drunen, *Electrochem. Sci. Technol.*, 1980, **127**, 1655–1659.
42 P. Claes, B. Thirion and T. Glibert, *Electrochim. Acta*, 1996, **41**, 141–146.
43 Y. Kanai, K. Fukunaga, K. Terasaka and S. Fujioka, *Chem. Eng. Sci.*, 2013, **100**, 153–159.
44 S. Frangini and S. Scaccia, *J. Electrochem. Soc.*, 2004, **2**, 1251–1256.
45 V. A. Volkovich, T. R. Gri, D. J. Fray and R. C. Thied, *J. Nucl. Mater.*, 2000, **282**, 152–158.
46 W. R. Carper, P. G. Wahlbeck and T. R. Griffiths, *J. Phys. Chem. B*, 2012, **116**, 5559–5567.
47 J. J. Tong, X. L. Lei, J. Fang, M. F. Han and K. Huang, *J. Mater. Chem. A*, 2016, **4**, 1828–1837.
48 S. Frangini and S. Scaccia, *Int. J. Hydrogen Energy*, 2014, **39**, 12266–12272.
49 M. Cassir, G. Moutiers and J. Devynck, *J. Electrochem. Soc.*, 1993, **140**, 3114–3122.
50 D. Corradini, F. Coudert and R. Vuilleumier, *Nat. Chem.*, 2016, **8**, 454–460.
51 L. Zhang, X. Huang, C. Qin, K. Brinkman, Y. Gong, S. Wang and K. Huang, *Phys. Chem. Chem. Phys.*, 2013, **15**, 13147–13152.
52 P. J. Bruna, F. Grein and J. Passmore, *Can. J. Chem.*, 2011, **89**, 671–687.
53 A. Evans, W. Xing and T. Norby, *J. Electrochem. Soc.*, 2015, **162**, 1135–1143.
54 W. Xing, Z. Li, T. Peters, M. Fontaine, M. Mccann, A. Evans, T. Norby and R. Bredesen, *Sep. Purif. Technol.*, 2019, **212**, 723–727.
55 W. Xing, T. Peters, M. L. Fontaine, A. Evans, P. P. Henriksen, T. Norby and R. Bredesen, *J. Memb. Sci.*, 2015, **482**, 115–119.
56 M. R. Cerón, L. S. Lai, A. Amiri, M. Monte, S. Katta, J. C. Kelly, M. A. Worsley, M. D. Merrill, S. Kim and P. G. Campbell, *J. Memb. Sci.*, 2018, **567**, 191–198.
57 S. G. Patrício, E. Papaioannou, G. Zhang, I. S. Metcalfe and F. M. B. Marques, *J. Memb. Sci.*, 2014, **471**, 211–218.
58 G. J. Janz and N. P. Bansal, *J. Phys. Chem. Ref. Data*, 1982, **11**, 507–693.
59 A. Ottochian, C. Ricca, F. Labat and C. Adamo, *J. Mol. Model.*, 2016, **22**, 1–8.
60 D. L. Roest, P. Ballone, D. Bedeaux and S. Kjelstrup, *J. Phys. Chem. C*, 2017, **121**, 17827–17847.
61 L. Malavasi, C. A. J. Fisher and M. S. Islam, *Chem. Soc. Rev.*, 2010, **39**, 4370–4387.
62 T. T. Norton, J. Ortiz-Landeros and Y. S. Lin, *Ind. Eng. Chem. Res.*, 2014, **53**, 2432–2440.
63 J. Ortiz-Landeros, T. Norton and Y. S. Lin, *Chem. Eng. Sci.*, 2013, **104**, 891–898.
64 L. Zhang, Y. Gong, J. Yaggie, S. Wang, K. Romito and K. Huang, *J. Memb. Sci.*, 2014, **453**, 36–41.
65 J. Tong, F. Si, L. Zhang and J. Fang, *Chem. Commun.*, 2015, **51**, 2936–2938.
66 Y. Li, Z. Rui, C. Xia, M. Anderson and Y. S. Lin, *Catal. Today*, 2009, **148**, 303–309.
67 L. Gao, J. Robert Selman and P. Nash, *J. Electrochem. Soc.*, 2018, **165**, 324–333.
68 M. S. Khan, M. S. Islam and D. R. Bates, *J. Mater. Chem.*, 1998, **8**, 2299–2307.
69 M. J. D. Rushton and A. Chroneos, *Sci. Rep.*, 2014, **4**, 1–6.
70 C. Zhang, J. Sunarso and S. Liu, *Chem. Soc. Rev.*, 2017, **46**, 2941–3005.
71 S. J. Skinner and J. A. Kilner, *Mater. Today*, 2003, **6**, 30–37.
72 K. Eguchi, T. Setoguchi, T. Inoue and H. Arai, *Solid State Ionics*, 1992, **52**, 165–172.

73 X. Wang, Y. Ma, S. Li, A. H. Kashyout, B. Zhu and M. Muhammed, *J. Power Sources*, 2011, **196**, 2754–2758.
74 P. Shuk, H.-D. Wiemhofer, U. Guth, W. Gopel and M. Greenblatt, *Solid State Ionics*, 1996, **89**, 179–196.
75 Z. Rui, M. Anderson, Y. Li and Y. S. Lin, *J. Memb. Sci.*, 2012, **417–418**, 174–182.
76 S. J. Chung, J. H. Park, D. Li, J. I. Ida, I. Kumakiri and J. Y. S. Lin, *Ind. Eng. Chem. Res.*, 2005, **44**, 7999–8006.
77 P. Biedenkopf, M. M. Bischoff and T. Wochner, *Werkstoffe und Korrosion*, 2000, **51**, 287–302.
78 G. J. Janz, A. Conte and E. Neuenschwander, *Corros. - Natl. Assoc. Corros. Eng.*, 1963, **19**, 292–294.
79 N. Xu, X. Li, M. A. Franks, H. Zhao and K. Huang, *J. Memb. Sci.*, 2012, **401–402**, 190–194.
80 J. M. Fisher and P. S. Bennett, *J. Mater. Sci.*, 1991, **26**, 749–755.
81 R. L. Lehman, J. S. Gentry and N. G. Glumac, *Thermochim. Acta*, 1998, **316**, 1–9.
82 P. Zhang, J. Tong, Y. Jee and K. Huang, *Chem. Commun.*, 2016, **52**, 9817–9820.
83 A. S. Bhalla, R. Guo and R. Roy, *Mater. Res. Innov.*, 2000, **4**, 3–26.
84 X. Dong, W. Jin, N. Xu and K. Li, *Chem. Commun.*, 2011, **47**, 10886–10902.
85 Y. Teraoka, H.-M. Zhang, S. Furukawa and N. Yamazoe, *Chem. Lett.*, 1985, **14**, 1743–1746.
86 M. Anderson and Y. S. Lin, *J. Memb. Sci.*, 2010, **357**, 122–129.
87 X. Tan, N. Liu, B. Meng, J. Sunarso, K. Zhang and S. Liu, *J. Memb. Sci.*, 2012, **389**, 216–222.
88 T. T. Norton and Y. S. Lin, *Solid State Ionics*, 2014, **263**, 172–179.
89 X. Jiang, J. Zhu, Z. Liu, S. Guo and W. Jin, *Ind. Eng. Chem. Res.*, 2016, **55**, 3300–3307.
90 O. Ovalle-Encinia, H. Pfeiffer and J. Ortiz-Landeros, *J. Memb. Sci.*, 2018, **547**, 11–18.
91 O. Ovalle-Encinia, H. Pfeiffer and J. Ortiz-Landeros, *Ind. Eng. Chem. Res.*, 2018, **57**, 9261–9268.
92 B. F. K. Kingsbury and K. Li, *J. Memb. Sci.*, 2009, **328**, 134–140.
93 H. Huang, S. Cheng, J. Gao, C. Chen and J. Yi, *Mater. Lett.*, 2014, **137**, 245–248.
94 X. Dong, J. Ortiz Landeros and Y. S. Lin, *Chem. Commun.*, 2013, **49**, 9654–9656.
95 R. M. Khattab, M. M. S. Wahsh and N. M. Khalil, *Ceram. Int.*, 2012, **38**, 4723–4728.
96 S. Li, C. A. Wang and J. Zhou, *Ceram. Int.*, 2013, **39**, 8833–8839.
97 L. Zhang, N. Xu, X. Li, S. Wang, K. Huang, W. H. Harris and W. K. S. Chiu, *Energy Environ. Sci.*, 2012, **5**, 8310–8317.
98 L. Zhang, X. Li, S. Wang, K. G. Romito and K. Huang, *Electrochem. commun.*, 2011, **13**, 554–557.
99 J. Fang, J. Tong and K. Huang, *J. Memb. Sci.*, 2016, **505**, 225–230.
100 J. Fang, N. Xu, T. Yang, P. Zhang, J. Tong and K. Huang, *J. Memb. Sci.*, 2017, **523**, 439–445.
101 L. Zhang, Y. Gong, K. S. Brinkman, T. Wei, S. Wang and K. Huang, *J. Memb. Sci.*, 2014, **455**, 162–167.
102 L. Zhang, J. Tong, Y. Gong, M. Han, S. Wang and K. Huang, *J. Memb. Sci.*, 2014, **468**, 373–379.
103 X. Tan, Z. Wang and K. Li, *Ind. Eng. Chem. Res.*, 2010, **49**, 2895–2901.
104 A. Gouveia Gil, Z. Wu, D. Chadwick and K. Li, *Ind. Eng. Chem. Res.*, 2015, **54**, 5563–5571.
105 M. Zuo, S. Zhuang, X. Tan, B. Meng, N. Yang and S. Liu, *J. Memb. Sci.*, 2014, **458**, 58–65.
106 S. Zhuang, Y. Li, M. Zuo, X. Tan, B. Meng, N. Yang and S. Liu, *Sep. Purif. Technol.*, 2014, **132**, 712–718.
107 B. Lu and Y. S. Lin, *Ind. Eng. Chem. Res.*, 2014, **53**, 13459–13466.
108 X. Dong, H. C. Wu and Y. S. Lin, *J. Memb. Sci.*, 2018, **564**, 73–81.
109 Z. Rui, M. Anderson, Y. S. Lin and Y. Li, *J. Memb. Sci.*, 2009, **345**, 110–118.
110 E. I. Papaioannou, H. Qi and I. S. Metcalfe, *J. Memb. Sci.*, 2015, **485**, 87–93.
111 P. Zhang, J. Tong and K. Huang, *J. Mater. Chem. A*, 2017, **5**, 12769–12773.
112 T. T. Norton, B. Lu and Y. S. Lin, *J. Memb. Sci.*, 2014, **467**, 244–252.
113 M. L. Fontaine, T. A. Peters, M. T. P. McCann, I. Kumakiri and R. Bredesen, *Energy Procedia*, 2013, **37**, 941–951.
114 J. Tong, L. Zhang, M. Han and K. Huang, *J. Memb. Sci.*, 2015, **477**, 1–6.
115 J. Tong, L. Zhang, J. Fang, M. Han and K. Huang, *J. Electrochem. Soc.*, 2015, **162**, 2015–2018.
116 Z. Yang, Y. Zhu and M. Han, *J. Alloys Compd.*, 2017, **723**, 70–74.
117 S. G. Patrício, E. I. Papaioannou, B. M. Ray, I. S. Metcalfe and F. M. B. Marques, *J. Memb. Sci.*, 2017, **541**, 253–261.
118 R. Lan, S. M. M. Abdallah, I. A. Amar and S. Tao, *J. Memb. Sci.*, 2014, **468**, 380–388.
119 Li, Q. Borup, F. ; Petrushina, I. ; Bjerrum, Niels J, L. Qingfeng, F. Borup, I. Petrushina and N. J. Bjerrum, *J. Electrochem. Soc.*, 1999, **146**, 2449–2454.
120 J. L. Wade, K. S. Lackner and A. C. West, *Solid State Ionics*, 2007, **178**, 1530–1540.
121 R. Balasubramanian and S. Chowdhury, *J. Mater. Chem. A*, 2015, **3**, 21968–21989.
122 G. M. Pressouyre and F. M. Faure, *Hydrogen embrittlement: prevention and control.*, 1988.
123 O. I. Radkevych and H. V. Chumalo, *Mater. Sci.*, 2003, **39**, 596–600.
124 T. E. Graedel, J. P. Franey, G. J. Gualtieri, G. W. Kammlott and D. L. Malm, *Corros. Sci.*, 1985, **25**, 1163–1180.
125 M. B. Mitchell, V. N. Sheinker and M. G. White, *J. Phys. Chem.*, 1996, **100**, 7550–7557.
126 Y. Liu, W. Cen, Z. Wu, X. Weng and H. Wang, *J. Phys. Chem. C*, 2012, **116**, 22930–22937.
127 T. Chen, H. C. Wu, Y. Li and Y. S. Lin, *Ind. Eng. Chem. Res.*, 2017, **56**, 14662–14669.
128 T. Chen, B. Yu, Y. Zhao, Y. Li and Y. S. Lin, *J. Memb. Sci.*, 2017, **540**, 477–484.
129 J. Gao, L. Li, Z. Yin, J. Zhang, S. Lu and X. Tan, *J. Memb. Sci.*,

View Article Online
DOI: 10.1039/C9TA01979K

2014, 455, 341–348.
130 Y. Alqaheem, A. Thursfield, G. Zhang and I. S. Metcalfe, *Solid State Ionics*, 2014, **262**, 262–265.
131 D. P. Harrison, *Ind. Eng. Chem. Res.*, 2008, **47**, 6486–6501.
132 X. Dong and Y. S. Lin, *J. Memb. Sci.*, 2016, **520**, 907–913.
133 M. Anderson and Y. S. Lin, *AIChE J.*, 2013, **59**, 2207–2218.
134 P. Zhang, J. Tong and K. Huang, *ACS Sustain. Chem. Eng.*, 2016, **4**, 7056–7065.
135 P. Zhang, J. Tong and K. Huang, *ACS Sustain. Chem. Eng.*, 2017, **5**, 5432–5439.
136 S. R. Alexander and J. Winnick, *J. Appl. Electrochem.*, 1994, **24**, 1092–1101.
137 A. Burke, J. Winnick, C. Xia and M. Liu, *J. Electr*, 2002, **149**, 160–166.
138 S. R. Alexander and J. Winnick, *AIChE J.*, 1994, **40**, 613–620.
139 M. Franke and J. Winnick, *Ind. Eng. Chem. Res.*, 1989, **28**, 1352–1357.
140 K. Scott and J. Winnick, *Gas Sep. Purif.*, 1988, **2**, 23–27.
141 D. J. McHenry and J. Winnick, *AIChE J.*, 1994, **40**, 143–151.
142 J. Bartling and J. Winnick, *J. Electrochem. Soc.*, 2003, **150**, 99–107.
143 J. Johnson and J. Winnick, *Sep. Purif. Technol.*, 1999, **15**, 223–229.
144 C. N. Wauters and J. Winnick, *AIChE J.*, 1998, **44**, 2144–2148.
145 C. N. Wauters and J. Winnick, *J. Electrochem. Soc.*, 1996, **143**, 5–6.
146 K. Zhang, X. S. Li, W. Z. Li, A. Rohatgi, Y. Duan, P. Singh, L. Li and D. L. King, *Adv. Mater. Interfaces*, 2014, **1**, 1400030–1.
147 T. Harada, F. Simeon, E. Z. Hamad and T. A. Hatton, *Chem. Mater.*, 2015, **27**, 1943–1949.
148 L. Huang, C. Xu, R. Ren, Q. Zheng, Z. Wang, B. Louis and Q. Wang, *Sustain. Energy Fuels*, 2018, **2**, 68–72.
149 W. Gao, T. Zhou, Y. Gao, B. Louis, D. O'Hare and Q. Wang, *J. Energy Chem.*, 2017, **26**, 830–838.
150 R. Anantharaman, T. Peters, W. Xing and M. Fontaine, *Faraday Discuss.*, 2016, **192**, 251–269.
151 S. R. Sherman, J. R. Gray, K. S. Brinkman and K. Huang, *J. Memb. Sci.*, 2012, **401–402**, 323–332.
152 J. Fang, X. Jin and K. Huang, *J. Memb. Sci.*, 2017, **549**, 142–150.

View Article Online
DOI: 10.1039/C9TA01979K

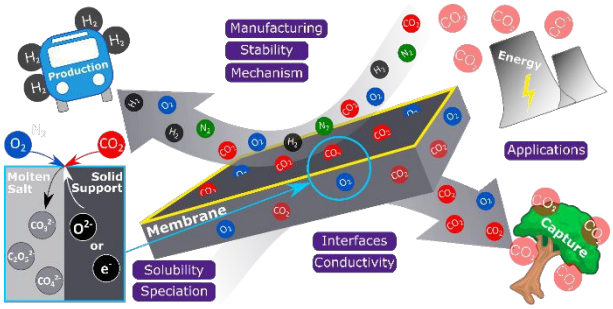

First review of supported molten-salt membranes highlighting materials challenges, mechanistic development and manufacturing opportunities towards energy applications.